University of Cape Town

Masters Thesis

Evaluating global ocean reanalysis systems for the greater Agulhas Current System

Author:
Kyle Cooper

Supervisors:
Dr. Bjorn Backeberg
Dr. Juliet Hermes
Dr. Julie Deshayes
Dr. Jennifer Veitch

A thesis submitted in fulfilment of the requirements
for the degree of Master of Science

in the

Department of Oceanography

November 2014

Declaration of Authorship

I, Kyle Cooper, declare that this thesis titled, 'Evaluating global ocean reanalysis systems for the greater Agulhas Current System' and the work presented in it are my own. I confirm that:

- This work was done wholly or mainly while in candidature for a research degree at this University.
- Where any part of this thesis has previously been submitted for a degree or any other qualification at this University or any other institution, this has been clearly stated.
- Where I have consulted the published work of others, this is always clearly attributed.
- Where I have quoted from the work of others, the source is always given. With the exception of such quotations, this thesis is entirely my own work.
- I have acknowledged all main sources of help.
- Where the thesis is based on work done by myself jointly with others, I have made clear exactly what was done by others and what I have contributed myself.

Signed: _____

Date: _____

"Everything should be made as simple as possible, but not simpler"

Albert Einstein

UNIVERSITY OF CAPE TOWN

Abstract

Faculty of Science
Department of Oceanography

Master of Science

Evaluating global ocean reanalysis systems for the greater Agulhas Current System

by Kyle Cooper

Operational oceanography aims to accurately hindcast and forecast the state of the ocean. An international initiative, the Global Ocean Data Assimilation Experiment (GODAE), developed and increased the capacity for global operational oceanography. However, the products from the global initiatives were regionally inapplicable due to low spatial resolutions, and have recently improved through GODAE OceanView. A number of local operational oceanographic initiatives have been setup over the southern African regional ocean, but proved to be unsustainable and ended. Recently, the aim to develop a regional ocean prediction system has arisen, and initial steps have been taken. This thesis aims to address the lack of local capacity in operational oceanography, and contribute to a crucial process in developing a regional ocean prediction system. Here, we validate and investigate the the differences between three global reanalysis products, namely MyOcean (GLORYS2V1), HYCOM (U.S Naval Research Laboratory) and BlueLINK (OFAM3). These reanalysis products are validated and investigated over the greater Agulhas Current System, which is a crucial system in Southern African regional ocean. The salient oceanographic features represented in the reanalysis products are initially compared to historical literature of the region and followed by available unassimilated observations (i.e independent). The results show that the reanalysis products from MyOcean, and the U.S Naval Research Laboratory satisfactorily simulate the major salient oceanographic features of the Agulhas Current System. Bluelink does not correctly portray the structure of the source and retroflection regions, and therefore has limited use over the Agulhas Current System. The differences between the three products indicates that the data assimilate does not sufficiently constrain the models in order for their solutions over the Agulhas System to converge. The evaluation of these global ocean reanalysis products is a critical step toward a regional ocean prediction system over Southern Africa, and building toward the local capacity to accomplish this goal.

Acknowledgements

This work would not be possible without the guidance and tutelage of my four supervisors: Dr Bjorn Backeberg, Dr Juliet Hermes, Dr Julie Deshayes and Dr Jennifer Veitch. Bjorn, I will never forget, having a beer and Peking duck in a back alley restaurant in Bejing. I am grateful for pushing me to be a better scientist, but also providing much needed support and encouragement that never went unnoticed. Juliet, the doors you opened and opportunities you created were life changing and I never thought possible. I am grateful for all the scientific advice and subtle corrections in my work that had a significant impact and was dearly missed for a few months. Julie, the afternoon conversations, scientific or not, were inspirational and enjoyable. I am indebted to the technical assistance, that you not only passed onto myself, but also getting down in the trenches fighting the errors with me. Jenny, your critical and objective view to this work was unique and essential. Your honest feedback was always appreciated and kept me on my toes. Bjorn, Juliet, Julie and Jenny, though this journey has ended it has been incredible and I am indebted the inspiration,knowledge, advice, experience, expertise and support you have given me. I am very grateful, thank you.

My sincere thanks go to Dr James Richman and Dr Jeffrey Book for hosting myself at the Naval Research Laboratory and for showing me the Southern United States. Jeff, the technical expertise and scientific knowledge I acquired under your tutelage while at the NRL has been essential not only to this work, but also myself as a budding scientist. Jim, without the hard work of yourself and your team, this work would have been significantly emptier without the HYCOM data. I am grateful to Dr Mark Mathews for reviewing this work with an objective eye.

I am thankful to Prof. Harry Bryden for the use of the Agulhas Current Experiment data, Prof. Herman Ridderinkhof for the access to the LOCO data, and Dr Marjolaine Krug for the ASAR data. The access to these independent datasets played a critical part to this research, and would not be possible without it. I am grateful to Dr Gary Brassington and Dr Duane Beckett for processing and access to the Bluelink data.

I gratefully acknowledge the National Research Foundation, and the South African Environmental Observation Network (SAEON) for the funding of this research. I am thankful to the Nansen - Tutu Centre, SAEON, Office of Naval Research and ICE-MASA for travel funding.

I would like to thank the friends who supported me throughout this work: Marcel, Laura, Jen, Chris, Shane, Terrence, Nic and Tess. The tea crew of Daniel,Isabelle, Luke and Raissa for intelligent, and entertaining times in the department. Neil, the memories in Hawaii will not be easily forgotten and more will have to be made in the future.

Lastly I would like to thank my family who supported me through my successes, failures, frustrations, and triumphs. Rob, Pam and Dylan, without your love and support this work would not be possible and I am extremely lucky to have had you behind me in this journey.

Contents

List of Figures

List of Tables

Chapter 1

Introduction

A new division in operational oceanography was birthed out of the possibility to produce a global ocean prediction system, similar to existing atmospheric weather prediction systems. To determine the feasibility of creating global ocean prediction systems, the Global Ocean Data Assimilation Experiment (GODAE) was formed in 1997. GODAE was an international co-operation initiative mandated to develop forecasting capabilities for the global ocean (Smith and Lefèbvre, 1997).

GODAE defined operational oceanography as 'the processing is done in a routine and regular way, with pre-determined systematic approach and constant monitoring and performance' (International GODAE Steering Team, 2000). This definition emphasizes a high quality of service both scientifically and technically, which are constantly maintained, having predictable delivery of products (Schiller and Brasssington, 2011).

GODAE was the pilot project which tested the feasibility of setting up global ocean prediction systems and developing the capacity to be able to build and run ocean prediction systems (Smith and Lefèbvre, 1997). A number of global prediction systems are operational, having been developed and implemented through GODAE (Schiller and Brasssington, 2011). The products from these prediction systems are readily available, being produced with numerical models that are routinely assimilated with satellite and available *in-situ* observations. The setup, development, and running of these global prediction systems fulfilled the aims of GODAE, which ended in 2008. The ending of GODAE left a number of challenges, but in particular many of the prediction systems were unable to run global simulations at eddy permitting spatial resolutions due to the computational cost and run time (Schiller and Brasssington, 2011).

GODAE OceanView aimed to address the challenges left unaddressed in GODAE, with the major challenge being to improve the accuracy and availability of forecast products

from the current operational prediction systems (Traon et al., 2009). Through the establishment of GODAE OceanView in 2009, many of the prediction systems have significantly improved their configurations, accuracy and assimilation of data in their forecast products (Schiller and Brasssington, 2011). A notable improvement is that a number of the operational prediction systems that currently have the ability to run global simulations at eddy permitting horizontal resolutions, and a few systems at eddy resolving resolutions. The ability of these forecast models to resolve mesoscale and sub-mesoscale scales features is essential to the accuracy of the forecast product and important when considering the applications (Schiller and Brasssington, 2011).

Oceanic forecasts products have a number of applications that depend on different spatial and temporal scales. The first type of product is a forecast, usually on a short (daily) to medium (weekly) time scale, and have a number of applications. Schiller and Brasssington (2011) investigated an upwelling event off the Bonney Coast in South Australia and identified potential users and applications such as: search and rescue, marine accident and emergencies, defense, fisheries management, and marine management (assisting in policy and decision making). Industries that can use these products include: offshore oil and gas, ship routing, renewable energy, weather, wave, and ecosystem forecasting. Coastal applications could include: management of ports, bilge discharge, coastal surge, recreational fishing, diving, swimming, and sailing.

The second type of product is a hindcast or reanalysis, which spans a number of years into the past. The reanalysis products are mainly used to evaluate the accuracy of the prediction system's products, but also troubleshoot, identify problems, qualitatively understand the dynamics, and provide initial conditions for forecasting (Schiller and Brasssington, 2011).

The need for a prediction system for Southern Africa was first realized and addressed in 2003 with the establishment of the regional ocean prediction system (ROPes), but ended up facing a number of issues and proved to be unsustainable. The first African operational oceanographic meeting was held in 2009, and the OceanSAfrica initiative was launched in 2012 (OceanSAfrica, 2012).

OceanSAfrica aimed to address the needs of the offshore industries such as oil and gas, the South African Navy, the insurance industry, ecosystem modeling, research, marine leisure activities, harmful algal blooms, and management of marine resources (Veitch et al., 2010; van Ballegooyen et al., 2011). OceanSAfrica consisted of four pillars: remote sensing, *in-situ* observations, ocean modeling, and data dissemination. The responsibility of these four pillars was split among multiple institutions with ocean modeling falling under SimOcean.

SimOcean was tasked to setup and develop an operational oceanographic prediction system and continually develop the products. This was the first real attempt at a fully operational system over Southern Africa, but once again proved to be unsustainable due to lack of funding. Consequently a regional oceanographic prediction system still was undeveloped and not operational in South Africa (OceanSAfrica, 2012; Veitch et al., 2010).

The motivation to produce a regional prediction product is well defined having a number of defined applications mentioned above. Backeberg et al. (2014) is the first step toward the development of a regional prediction system, but numerous challenges are still to be addressed. As the system is still in its infancy there is still room for further development for improvement of the free running model, further assimilation of observations, and improved boundary conditions. However the simulation produced by Backeberg et al. (2014) is not operational as defined above, and therefore no local organisation currently provides a regional oceanographic forecast. This means that operational oceanographic predictions are obtained from existing global prediction systems.

At the ending of GODAE, these global prediction systems had a spatial resolution that was too coarse and unable to correctly resolve the unique dynamics around Southern Africa. Continued development of the global prediction systems, through GODAE OceanView, has increased the resolution (eddy resolving/permitting), and coverage (regional/global). These improvements allow for the application of products from global prediction systems over the southern African region. A number of institutions that run global prediction systems (Mercator Ocean, U.S Navy, and BlueLINK>) have made their reanalysis products available to the South African research community.

1.1 Objectives

The first aim of this thesis is to validate the global prediction products provided by Mercator Ocean, the U.S Navy, and BlueLINK> using independent observations, and current literature of greater Agulhas Current System. The Agulhas Current is a key system in the southern Africa region, which is difficult to correctly simulate (Penven et al., 2011), impacts global climate (Beal et al., 2011), and is environmentally and economically important for South Africa (Veitch et al., 2010). Therefore the validation of these global reanalysis products will allow them to be used as boundary conditions for a nested regional simulation (Backeberg et al., 2014), and a validation method for future assimilated products.

The second aim of this thesis is to investigate the ability of assimilated observations to constrain the numerical model in the global prediction products in Mercator Ocean and the U.S Navy. A convergence of reanalysis products will indicate the ability of data assimilation to constrain the reanalysis products, across different numerical model configurations and data assimilation schemes. A divergence would indicate that the reanalysis products cannot be constrained through data assimilation.

Chapter 2

Literature Review

2.1 Prediction systems

Global prediction systems require a number of components, across an array of different disciplines. The fundamental components of a prediction system are: observations that provide near real-time data input, a numerical model with a unique configuration and forcing field, and an efficient data assimilation scheme. These will be further discussed below, but there are a number of other essential components required to run an operational prediction system. Monitoring of quality in product generation, research and development of the system, involvement of users and dissemination of data, high performance computing, and data storage are components that are not discussed in this thesis.

2.1.1 *In-situ* observations

A large array of real time and delayed time observations are used in global prediction systems. Conductivity-Temperature-Depth (CTD) profiles are gathered from a number of different sources, which include: Argo floats, gliders, ships and mooring lines. Argo floats have currently reached a density of 3°x 3°of the global ocean with over 3000 floats. This was the goal of the Argo program, and provides CTD profiles in real-time every ten days (Argo Science Team, 2001). Gliders are similar to Argo floats as they provide both real time and delayed time CTD profiles depending on the objective of its mission, but they can be steered unlike Argo floats which are Lagrangian. A number of mooring arrays such as the TAO/TRITON, PIRATA, and RAMA (Mcphaden et al., 2009) provide real-time CTD profiles of the equatorial tropical ocean. Finally temperature profiles of

eXpandable Bathy-Thermographs (XBT) from volunteer vessels that run on specific routes report in real-time, but are limited in the temporal extent (Goni et al., 2009).

2.1.2 Satellite observations

Sea surface temperatures and altimetry observed from satellites are vital inputs to a prediction system. SST is the most observed oceanic variable by both geostationary, and polar orbiting satellites. SST observed from geostationary satellites is generally of a course resolution covering a wide swath, while polar orbits have improved spatial resolution and accuracy, but lower observational frequency (Schiller and Brasssington, 2011). SST products are then created from these two satellite orbits. Satellite altimetry can observe a vast array of dynamical processes, through the sea surface height (SSH), in the ocean such as: tides, wind, waves, swell and eddies (Schiller and Brasssington, 2011). Currently there are a number of different satellite missions observing SSH with different configurations, corrections and orbits, which are all essential to prediction systems (Schiller and Brasssington, 2011).

2.1.3 Numerical model

Ocean general circulation models (further referred to as a numerical model) solve an extension of the Navier-Stokes equations for a thin layer on a rotating planet (Stewart, 2008). The ocean state equation is based on temperature, salinity and pressure and assumes that the ocean is incompressible and hydrostatic to simplify the calculation of these equations (Schiller and Brasssington, 2011). There are a number of configurations within numerical models that uniquely define them such as: the model code, eddy resolving ability (i.e. spatial resolution), coastal and bathymetric control, boundary conditions, numerical methods, computational performance, and turbulent parameterisations (Schiller and Brasssington, 2011). As these configurations vary significantly there are a number of different numerical model configurations used by global prediction systems.

2.1.4 Data assimilation

The primary purpose and aim of data assimilation is to provide the best possible estimate of the ocean state at a given time using a combination of both numerical models, and observations (Oke, 2002; Schiller and Brasssington, 2011). This best estimate of the ocean state is assumed to lie somewhere between the numerical model, and the

observations. Ideally, when sufficient observations are available, they are used as a constraining term in the forecast simulation, but where the observations are erroneous only the numerical model is used (Oke, 2002).

Data assimilation aims to achieve a balance between the observations and the numerical model, by weighting each component depending on their error estimates (Schiller and Brasssington, 2011). This weighting determines which component, the numerical model or the observations, is relied upon more. Three typical situations arise when determining which component will be relied upon, depending on the error estimate and the spatial distribution of the observational data.

When the observational data is sparse (i.e. scattered irregularly in space on the model grid) the missing values are filled by interpolating between observed data points. The interpolation must take into account the measurement error in the interpolated values, as this would impact the weighting of the two components during assimilation.

When the observational data is lacking in both space and time, the missing values are obtained by extrapolating the available observation until it no longer correlates with the numerical model (i.e remain consistent with numerical model)

When the observations are numerous, but possibly inaccurate, the values from both the observations, and the numerical model are smoothed, but weighted, so that either component is heavily depended on. If the observations are largely inaccurate, they will be omitted, and the numerical simulation will be used. In this case the weighting determined from the error estimate will rely more on the numerical model.

Various different assimilation schemes exist: variational, incremental 4D-Var, dual formulation, Kalman Filter, Model Reduction, and Ensemble methods (Schiller and Brasssington, 2011).

2.2 The greater Agulhas Current System

2.2.1 Surface features

The surface salient oceanographic features of the Agulhas Current system are described in detail by Lutjeharms (2006) and shown in (fig. 2.1). Below the major components of the Agulhas Current System are described in detail.

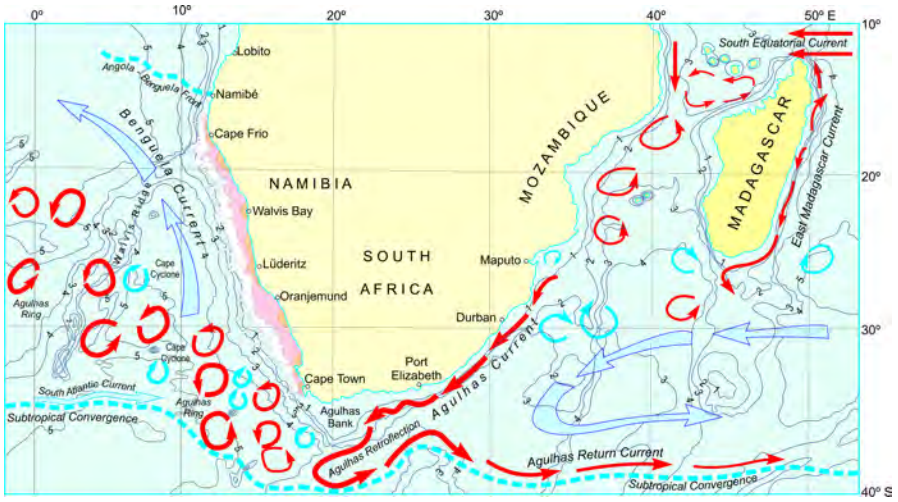

FIGURE 2.1: The major salient oceanographic features of the greater Agulhas Current system. The sources: Mozambique Channel eddies, East Madagascar eddies, and the Agulhas Current Recirculation. The stable northern Agulhas (Durban to Port Elizabeth), and variable southern Agulhas (Port Elizabeth onwards). The retroflection of the Agulhas Current, and its eastward continuation as the Agulhas Return Current meandering northward around the Agulhas Plateau. The eddy corridor of anti-cyclonic, and cyclonic eddies propagating from the retroflection region north-westward into the South Atlantic. Adapted from Ansorge and Lutjeharms (2007)

2.2.1.1 Source Regions

The South Equatorial Current flows westward until it reaches the east coasts of Africa and Madagascar. At the east coast of Africa, the South Equatorial Current splits, flowing northward and southward. At the east coast of Africa the southward branch flows through the Mozambique Channel. At the east coast of Madagascar the South Equatorial Current splits, flowing northward around the northern tip of Madagascar, and southward becoming the East Madagascar Current.

The flow through the Mozambique Channel occurs in the form of eddies, rather than a coherent current, which propagate into the main Agulhas Current (Sæ tre and Da Silva, 1984). The East Madagascar Current flows southward along the east coast of Madagascar as an intense western boundary current, but at a smaller scale. As the East Madagascar Current reaches the southern tip of Madagascar it retroflects creating cyclonic, and anti-cyclonic eddies that propagate into the Agulhas Current (Lutjeharms et al., 1981). The third source of the volume transport for the Agulhas Current System is the recirculation at depth of the Agulhas Return Current (Lutjeharms, 2006). The Mozambique Channel, the flow south of Madagascar, and the recirculation of the Agulhas Return Current form the three sources of the Agulhas Current System (fig. 2.1).

2.2.1.2 Agulhas Current

The Agulhas Current is split into the northern and southern Agulhas, both having markably different characteristics, and variability. The northern Agulhas Current forms at approx. 27°S, and flows southward along the narrow continental shelf growing in size and strength until approx. 33°S becoming the southern Agulhas Current. The path of the northern Agulhas Current is highly stable and can be found within 31 km of the coast 80% of the time (Gründlingh, 1983; Bryden et al., 2005). The only source of variability in the path of the northern Agulhas is due to the Natal Pulse (Lutjeharms, 2006). The Natal Pulse is believed to form at the Natal Bight, where the continental shelf is markably wider, creating a meander that pushes the Agulhas Current path offshore (Lutjeharms and Roberts, 1988).

The southern Agulhas Current starts at approx. 33°S, where the continental shelf of the Agulhas Bank widens as it separates from the coast, and the angle of the continental slope decreases. The change in bathymetry increases the instability of the Agulhas Current causing its path to meander significantly during its southwestward flow. The instability creates plumes and cyclonic eddies inshore of the Agulhas Current that were previously bounded by the continental shelf lying close to the coast (Lutjeharms, 2006). The southern Agulhas Current flows south-westward along the continental slope of the Agulhas Bank into the retroflection region, south of Cape Agulhas.

2.2.1.3 Agulhas retroflection

The Agulhas retroflection region lies south of the Agulhas Bank, where the retroflection loop is not geographically stationary. The retroflection loop forms as the southern Agulhas Current leaves the Agulhas Bank and turns back on itself, changing its direction to flow eastward becoming the Agulhas Return Current (Lutjeharms and Roberts, 1988).

Through the retroflection process, South Indian Ocean water is transported into the South Atlantic gyre via eddies and filaments (Lutjeharms, 2006). This transport of warm salty water from the South Indian Ocean gyre into the South Atlantic gyre is termed as Agulhas Leakage and is a possible driver of regional and global climate (Beal et al., 2011). The main process of Agulhas Leakage is through the spawning of large anti-cyclonic eddies, termed Agulhas Rings, that propagate north-westward into the South Atlantic (Schouten et al., 2002). The secondary mechanism of Agulhas Leakage is filaments that break off from the main Agulhas Current, near the retroflection region, which flow over the Agulhas Bank and into the Benguela Current (Lutjeharms and Cooper, 1996). The last mechanism that contributes to Agulhas Current Leakage is the propagation of cyclonic eddies, that have previously been overlooked (Hall and Lutjeharms, 2011)

2.2.1.4 Agulhas Return Current

The eastward flow leaving the Agulhas retroflection region, that has not contributed toward the Agulhas Leakage, is the Agulhas Return Current (Lutjeharms and Ansorge, 2001). The Agulhas Return Current lies adjacent to the Subtropical Front causing instabilities through current shear and creating mesoscale eddies. As the Agulhas Return Current flows eastward from the retroflection region it is steered by the bathymetry it encounters. The Agulhas Return Current meanders northward, around the Agulhas Plateau, returning to its original latitude on the eastern side of the plateau (Lutjeharms, 2006). This is the only major meander in the Agulhas Return Current, which becomes less as the as it flows eastward. Finally the position of the Agulhas Return Current progressively moves southward, as it flows eastward, into the South Indian Ocean (Lutjeharms and Ansorge, 2001).

2.2.2 Transport and velocity sections

A large number of transects have been extracted in various locations over the Agulhas Current System. Here, the key sections of the system are shown in fig. 2.2 and are described below.

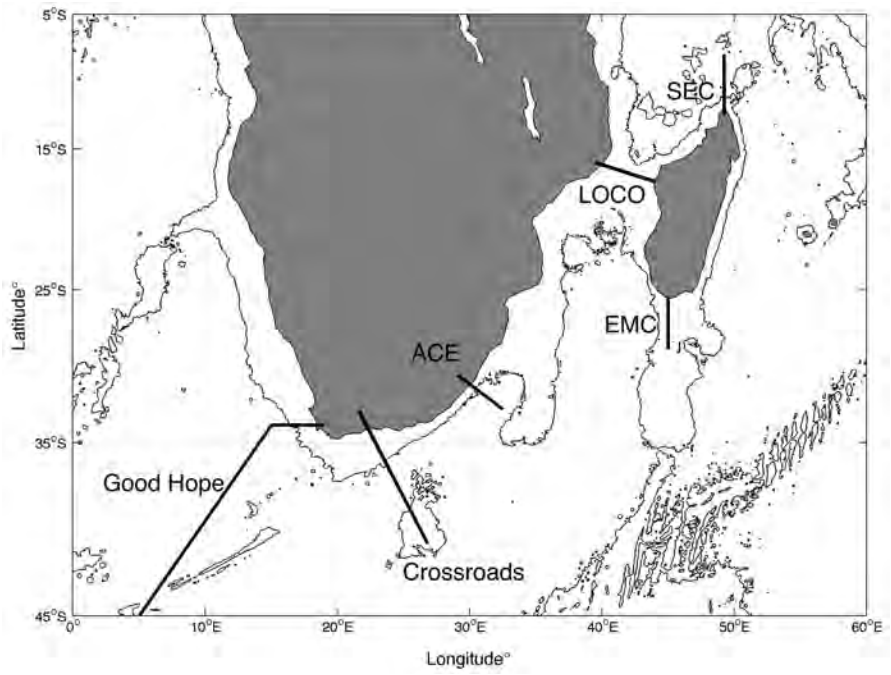

FIGURE 2.2: The locations of the six major transport sections extracted in the greater Agulhas Current system

2.2.2.1 LOCO

The Long-Term Ocean Climate Observations (LOCO) program set a mooring array through the narrowest part of the Mozambique Channel. The program started in 2003 to further investigate the results from Ridderinkhof and de Ruijter (2003). This study warranted further investigation of a possible northward extension of the Agulhas Undercurrent (Beal and Bryden, 1999), and the wide range of volume transports observed (Ridderinkhof et al., 2010).

This gave birth to the LOCO mooring line, which recorded data from 2003 to 2012 with the instruments being serviced at appropriate intervals with minimal technical failures. The details of the processing and calculations are described by Ridderinkhof et al. (2010). The mean volume transport is 16.7 Sv (southward), with a standard error of 3.1 Sv calculated from daily values ranging from 45.4 Sv (northward) to 67.2 Sv (southward). Seasonal, and interannual variability was investigated with a four year transport time series. The seasonal variability was found to be on the order of 4 Sv, with the interannual variability approx. 16 Sv (Ridderinkhof et al., 2010).

2.2.2.2 Agulhas Current Experiment (ACE)

The Agulhas Current Experiment took place between February and March 1995, and primarily focused on deploying an array of current meter moorings and full depth sections closely spaced to make a synoptic transport measurement. These moorings were recovered during the Agulhas Current Experiment Recovery and the same section repeated with CTD, and Lowered Acoustic Doppler Current Profiler (LADCP) observations (Beal and Bryden, 1999). Preliminary LADCP and geostrophic results for these cruises are discussed in Beal and Bryden (1997), which presents an Agulhas Current volume transport of 71 Sv, and a mean undercurrent of 10 cm/s.

This was then expanded by Beal and Bryden (1999), who described the overall structure of the Agulhas Current with the following features: V-shaped jet, velocities over 1.8 m/s, the core of the current 20km offshore, a width of 90 km between 50 cm/s isotachs, and the whole current found within 200 km of the shore. A full section volume transport of 73 Sv was calculated, and Beal and Bryden (1999) is the first study that includes the undercurrent in its volume transport calculation. The most prolific work from ACE was by Bryden et al. (2005) who measureed the strength, variability, mean structure and transport of the Agulhas Current. Daily sections from 5 March to 27 November 1995 of 2400 m depth and 203 km wide were taken to determine the structure and transport of the Agulhas Current.

The mean time section showed the following: the position of the Agulhas Current close to the continental shelf; the width of the current is 190 km; the Agulhas Undercurrent hugs the continental shelf below the 0 isotach; position of maximum velocity is above 300 m and 15 km offshore, while below 700 m the maximum velocity position is found 65 km offshore (Bryden et al., 2005). The mean total transport for the section is 69.7 ± 4.3 Sv (southward) with a range of 121.0 to 8.9 Sv (southward), while the "Jet" transport (sum of only the negative velocities) is 76.2 Sv (southward) with a range of 122.9 to 20.5 Sv (Bryden et al., 2005).

The undercurrent transport was calculated at 4.2 Sv, with a "Jet" transport (sum of only the positive values) of 6.5 Sv with a range of 26.5 Sv to 0.2 Sv. The offshore meandering observed by the mooring array was caused by five Natal pulses, which occurred between March 1995 and April 1996. These events each had a similar behavior pattern: the Agulhas Current weakened, a surfacing of the undercurrent with a northward flow over the continental slope, and finally the presence of cold waters (Bryden et al., 2005).

2.2.2.3 GoodHope Line

The GoodHope program established the GoodHope Line, which runs directly west of Cape Town until 15°E, then south-westward until 0°, and directly south (Ansorge et al., 2005). Due to the location of the GoodHope line it serves as a convenient location to measure the volume transport of Agulhas Leakage into the South Atlantic. The best observed estimate of Agulhas Leakage was calculated by Richardson (2007), who calculated the leakage from large anticyclonic eddies by following the trajectories of surface drifters, and RAFOS floats into the South Atlantic. About 25% of the floats and drifters were deemed to capture the Agulhas Leakage there by estimating a transport of 14 to 17 Sv.

A number of modeling studies have estimated the Agulhas Leakage using Eulerialan (van Sebille et al., 2009; Le Bars, 2014), or Lagrangian (Biastoch et al., 2009) methods or a combination of both (Loveday, 2014). Agulhas Leakage is problematic to measure correctly due to the high mesoscale variability and mixing in the Cape Basin (Boebel et al., 2003). This creates the challenge of separating the Agulhas Leakage from other water masses.

The use of simulated Lagrangian floats released upstream carrying a set transport value are counted as they cross the GoodHope line was used by a number of studies (Biastoch et al., 2009; van Sebille et al., 2009). However this method is extremely costly both computationally and temporally as discussed by Biastoch et al. (2009). van Sebille et al. (2010) determined two methods for measuring the Agulhas Leakage with Eulerian

sections, and reviewed the results with Lagrangian estimates, but the method needed to be tested before it could be applied to other model simulations. Loveday (2014) combined both Eulerian passive tracers, and Lagrangian virtual floats to determine the Agulhas Leakage.

Le Bars (2014) identified the boundary between the Agulhas Return Current and the Subtropical Front using satellite altimetry. This allowed for the volume transport difference to be calculated between the Agulhas Current and Agulhas Return Current to calculate the Agulhas Leakage anomalies. The method was developed using satellite altimetry and tested with INALT01 (Durgadoo et al., 2013), providing a method to measure Agulhas Leakage without having to deploy Lagrangian floats, and can be applied to course resolution climate models (Le Bars, 2014).

2.2.2.4 Crossroads

The Crossroads line is a recent observational line to measure yearly snapshots of the Agulhas Current, and the Agulhas Return Current on the annual Marion Island relief voyage (Ansorge, 2014). The Crossroads section lies in a unique location to measure both the Agulhas Current, and the Agulhas Return Current as they are both bathymetricaly constrained by the Agulhas Bank, and the Agulhas Plateau. The Crossroads section purposely coincides with the N198 altimetry track. Though the results of the hydrographic cruises cannot be directly compared in our study, we develop a method to estimate Agulhas Leakage, similar to Le Bars (2014), and the result is termed Westward Transport for this thesis.

2.3 Modeling the Agulhas Current System

A number of numerical models have been validated and utilized to investigate key processes in the greater Agulhas Current System : AGAPE (Biastoch and Krauss, 1999), SAfE (ROMS) (Penven et al., 2006), AG01-R (Biastoch et al., 2008), O4 (HYCOM) (Backeberg et al., 2009), INALT01 (Durgadoo et al., 2013), and AGIO and ARC112 (Loveday, 2014). A common problem among these numerical models is simulating the mean position of the retroflection region too far upstream, compared to observations, with a narrow pathway of eddies propagating into the South Atlantic (Penven et al., 2006; Backeberg et al., 2009). A number of numerical model simulations have corrected for this error by changing the numerical model configuration (Biastoch and Krauss, 1999; Biastoch et al., 2008).

Limited have combined numerical models with observations through data assimilation to investigate the Agulhas Current System (Backeberg et al., 2014).

A regional study of the Agulhas Current System by Backeberg et al. (2014) assimilated satellite altimeter along-track sea level anomaly data into a regional Hybrid Coordinated Model (Backeberg, 2008; Backeberg et al., 2009). The data assimilation was performed with the Ensemble Optimal Interpolation method, and showed a markably improved simulation of the Agulhas Current System. The simulation was validated with surface drifters and Argo profile floats, which improved the mesoscale dynamics, root mean square error of eddy kinetic energy, surface velocities, and the timing and placement of mesoscale features compared to surface drifters. However, the simulation misrepresented the Agulhas Return Current and sea surface temperatures (SST), which could be solved by either assimilating SST or improving the numerical model (Backeberg et al., 2014). Improving the numerical model is a better solution as it must be able to resolve the mesoscale dynamics and variability of the system before data is assimilated (Backeberg, 2008). This initial assimilation of sea level anomaly (SLA) is a first step to producing a prediction system tailored to the Agulhas Current System.

With the further development of a regional prediction product, the assimilation of additional datasets implies that there will be fewer independent datasets to validate these products. A validation method therefore needs to be developed with a fully operational prediction system. Global prediction products, which are assimilated with a large number of observational data sets, will be used to create a validation method using independent observational datasets and literature for the Agulhas Current System. This will create a robust and consistent method to evaluate future regional prediction products for the Agulhas Current System.

Chapter 3

Data and Methods

To address the objectives of this thesis, three global reanalysis products from established operational prediction systems are analyzed. The three products are acquired from the European forecasting center, MyOcean 2; the United States, Naval Research Laboratory; and the Australian, Commonwealth Scientific and Industrial Research Organization (CSIRO). For the remainder of this thesis, these global reanalysis products will be referred to as MyOcean (MyOcean 2), HYCOM (U.S NRL), and Bluelink (CSIRO). The configuration for each global reanalysis product is described below.

3.1 Numerical Model configuration

3.1.1 MyOcean

MyOcean was downloaded via ftp.myocean.mercator-ocean.fr under the product name GLOBAL_REANALYSIS_PHYS_001_009, which is produced by Mercator Ocean, the French contingent in MyOcean 2. MyOcean is run with NEMOv3.1 using the ORCA025_lim configuration, which sets a spatial resolution of 1/4°with 75 vertical levels (z-level) and forced by the ERA-interim atmospheric dataset (MyOcean, 2013). Here we use the reanalysis product GLORYS2v1, with monthly outputs from 1993 to 2009 of temperature, salinity, velocity, and sea surface height. Data is assimilated with the multi-data and multi-variate reduced order Kalman filter based on the Singular Extended Evolutive Kalman filter formulation and is applied using the increment analysis update (MyOcean, 2013). The observations assimilated include: delayed time along track satellite sea level anomaly, sea surface temperature, and *in-situ* profiles of temperature and salinity from the CORA3.1 database (MyOcean, 2013). MyOcean has been validated on a global

scale by Parent et al. (2013), showing good agreement with observations satisfactorily simulating the global variability.

3.1.2 HYCOM

The second global reanalysis product was obtained from the United States Naval Research Laboratory (NRL). HYCOM uses the HYbrid Coordinate Ocean Model (Bleck, 2002) at a spatial resolution of 1/12°with 32 vertical hybrid layers. The hybrid layers change the vertical coordinates depending on the depth in the water column. The surface layers use z-level coordinates, the bottom layers apply sigma coordinates, and isopycnic coordinates are utilized between the surface and bottom layers. HYCOM outputs daily values from 1993 to 2010 of temperature, salinity, sea surface height, and velocity, which is forced with NOGAPS (Metzger et al., 2014). Observations of sea surface height, sea surface temperature, sea ice concentration, *in-situ* observations from ships, buoys, XBTs, CTDs, gliders and Argo floats, are assimilated with the 3DVAR assimilation scheme (Cummings and Smedstad, 2013).

HYCOM is outputted as a daily product, and no monthly product is available. Therefore to make this product applicable to this thesis the daily outputs were averaged to monthly time steps at the NRL. Unfortunately an error was introduced to the velocity values in the isopycnic, and sigma layers. After timeous investigation no linear solution was found, and further investigation into the error falls beyond the scope of this thesis. This error was discovered in the latter part of the thesis and compromises have been made in the validation of this model, which is further discussed later.

3.1.3 Bluelink

Bluelink is produced using OFAM3 with version 4p1 configuration of the Modular Ocean Model (Oke et al., 2013). Bluelink is run at a spatial resolution of 1/10°with 51 vertical levels (z-star) forced by the ERA - interim atmospheric dataset (Oke et al., 2013). Bluelink produces daily outputs from 2000 to 2010 of temperature, salinity, velocity, sea surface height. Once again for the purpose of this thesis, the daily outputs were then averaged into monthly means. Bluelink has no assimilation.

3.2 Validation

To validate the three global reanalysis products described above, we compared MyOcean, HYCOM and Bluelink to unassimilated observations (i.e. independent), and knowledge

from current literature. The surface velocity, barotropic streamfunction, mean SSH and SSH variance are calculated to investigate if the major salient oceanographic features, and the variability of the Agulhas Current System are correctly simulated. Six key sections are taken throughout the greater Agulhas Current System (Figure 3.1) to investigate if the transport, and velocity of MyOcean, HYCOM and Bluelink are accurately simulated at depth. The description and processing of the above metrics are explained below.

3.2.1 Surface Velocity

The mean surface velocity for MyOcean, HYCOM, and Bluelink are plotted to include both the magnitude and direction. The magnitude is calculated from the vector velocity components from the first model layer, and averaged over the respective time period for each reanalysis product. Averaging the surface velocities over each simulation's time period; MyOcean (1993 to 2009), HYCOM (1993 to 2010) and Bluelink (2000 to 2010); instead of a common time period is to show the best possible structure and magnitude represented in each reanalysis product. The interannual variability between the respective time periods was checked and found to be negligible, allowing for the averaging of the different time periods. The colour bar limits (representing magnitude) are set to the reanalysis product with the smallest magnitude (i.e. MyOcean). The direction is shown by plotting the vector velocity components of each reanalysis product for magnitudes greater than 0.5 m/s.

Independent measurements of the surface velocities of the Agulhas Current System were derived from ASAR which uses the Doppler shift method from surface roughness measurements. . This method has been used to study the intensity, variability and structure of the Agulhas Current by Rouault et al. (2010). This data has been made available for this thesis and was used to independently validate the surface velocities of the MyOcean, HYCOM and Bluelink. The ascending, and descending modes from ASAR (2008 to 2009) are averaged to create a mean map of surface velocity over the Agulhas Current System. Before the ASAR surface velocities can be compared to the reanalysis products, the grid of each reanalysis product were linearly interpolated to match the ASAR grid. The increased spatial grids from MyOcean, HYCOM and Bluelink was averaged over the respective time period of ASAR, and the difference was calculated between the reanalysis products and ASAR.

3.2.2 Barotropic streamfunction

The barotropic streamfunction was calculated for MyOcean, HYCOM and Bluelink. The calculation of the barotropic streamfunction includes the velocity at depth, of which HYCOM was unusable, but in this case the HYCOM output included barotropic velocities. This allowed for the barotropic streamfunction to be calculated for HYCOM. The barotropic streamfunction calculation is described below:

The divergence equation for the barotropic velocities:

$$\frac{\partial U}{\partial x} + \frac{\partial V}{\partial y} = 0 \tag{3.1}$$

$$\text{Where} : U = \int_{-H}^{o} u dz \quad \text{and} \quad V = \int_{-H}^{o} v dz \tag{3.2}$$

Hence there exists a solution to the two equations:

$$\frac{\partial \Psi}{\partial y} = -U \qquad \frac{\partial \Psi}{\partial x} = -V \tag{3.3}$$

The constant for equation 3.3 is specified so that the barotropic streamfunction (Ψ) is set to zero over land. This calculation was performed for each time step of MyOcean (1993 to 2009), HYCOM (1993 to 2010) and Bluelink (2000 to 2010), and then averaged over time to give the mean barotropic streamfunction.

3.2.3 Surface Variability

The sea surface height is averaged for MyOcean, HYCOM and Bluelink for the respective time period of each reanalysis products. The standard deviation of SSH is calculated for MyOcean, HYCOM and Bluelink, and averaged over each reanalysis products respective time period. The mean standard deviation of SSH of HYCOM and Bluelink is then degraded to the common grid size (1/4°). The limits of the scalebar for the magnitude of SSH standard deviation are set to the reanalysis product with the smallest magnitude (i.e. MyOcean) for comparability. The 3000 m isobath for each respect reanalysis product is plotted over the mean SSH and mean SSH standard deviation.

The AVISO daily absolute dynamic topography (1993 to 2010) was downloaded from http://www.aviso.oceanobs.com/ and averaged into monthly time steps. The monthly absolute dynamic topography (1993 to 2010) was averaged, and the standard deviation calculated. The monthly mean absolute dynamic topography and standard deviation were plotted with the limits of the scalebar for the magnitude of standard deviation set to the reanalysis product with the smallest magnitude (i.e. MyOcean). Lastly the 3000

m isobath from ETOPO2v2 acquired from http://www.ngdc.noaa.gov/mgg/ was plotted with the mean and standard deviation of the mean absolute dynamic topography.

3.3 Section Validation

To validate the transport and velocity of MyOcean, HYCOM, and Bluelink at depth, six sections are extracted throughout the greater Agulhas System, shown in Figure 3.1.

Independent mooring data was made available at the LOCO, and ACE sections to independently validate MyOcean, HYCOM and Bluelink. To conserve the transport when comparing the reanalysis products a toolbox called: the physical analysis of gridded ocean data (PAGO) is employed. PAGO (http://www.whoi.edu/science/PO/pago/) is an inter-comparison tool for analyzing models with different grid sizes and grid type. PAGO provides a consistent method for interpolation across the different grid sizes minimizing errors such as large scale budget tracers (Deshayes et al., 2014). PAGO is applied to all three reanalysis products, and extracts the velocity and transport values over the six key sections in the Agulhas Current System. The transport values from MyOcean, HYCOM and Bluelink are initially compared to values from existing literature followed by an in-depth analysis from the *in-situ* moorings at the LOCO and ACE sections.

3.3.1 LOCO

The Long-Term Ocean Climate Observations (LOCO) program deployed and maintained a mooring array through the Mozambique Channel. The details of the program, and the method of the data processing followed are described by Ridderinkhof et al. (2010). For the purpose of this study, the daily transport values through the LOCO section from January 2004 to December 2009 have been averaged into monthly transport values.

A monthly transport time series of LOCO was plotted with the values from MyOcean, HYCOM, Bluelink, and the moorings for 2004 to 2009. The mean, standard deviation and correlation between each reanalysis product and the observations were calculated. The power density spectrum was calculated using 6 windows of the multi-taper method (Bronez, 1992) to determine the dominnant frequencies of the volume transport time series. The seasonal frequency was then removed from the transport time series, which was then plotted for 1993 to 2010. The seasonal frequency was removed by calculating a climatological mean and subtracting each time step, creating a volume transport

anomaly time series. The mean and standard deviation were calculated on this transport anomaly time series for the time period that is common between all three reanalysis products (2000 to 2009).

3.3.2 ACE

The Agulhas Current Experiment (ACE) investigated the Agulhas Current transport at 32°S with a mooring line of ADCPs and current meters from February to November 1995 (Bryden et al., 2005). The mooring data was initially obtained from the British Oceanographic Data Centre and had been processed through the initial stages as described in Bryden et al. (2005). However the daily data still needed to be gridded over the section, and averaged into monthly means. The daily data was gridded as described in Bryden et al. (2005) linearly interpreting the vertical grid at 20 m depth intervals, and the horizontal grid at 500 m length intervals. Finally the daily gridded data was averaged into monthly bins for February to November 1995.

The monthly volume transport values were extracted from MyOcean, and HYCOM with PAGO for the same time period of ACE, and the volume transport time series plotted. Unfortunately Bluelink does not cover this time period and was omitted from the transport time series. The mean, standard deviation and correlation between each reanalysis product and observations was computed. Lastly the transport time series of the reanalysis products, and the observations over the entire time period (1993 to 2010) were plotted and the mean and standard deviation were calculated over the common model time period (2000 to 2009).

3.3.3 Crossroads

The Crossroads section is based on the co-ordinates from the N198 altimetry track, and after the sections are extracted were checked against the satellite track co-ordinates. This needs to be done as PAGO uses the closest grid points to define the start and end co-ordinates of the section. This can change the angle of the section, and therefore the angle of flow through the north and west faces of the section. The angle of the flow needs to be accounted for, as the method to determine the boundaries of the current, is based on the dominant flow through the west faces of the section. Any small change in the angle of the section can cause errors in the method. Once the section is correctly extracted, we proceed to identify the boundaries of the Agulhas Current, and the Agulhas Return Current of each reanalysis product.

3.3.3.1 Boundary identification method

The method is primarily based on the high velocity values through the west faces of the sections as this was determined to be more dominant than the north faces. This was determined by plotting the velocity section of the north and west faces separately, which showed the west faces had higher velocities and number. Thus initially used the west faces to define the boundaries of the Agulhas Current and Agulhas Return Current. The north faces were then taken into account later on in the method.

The west face velocities are vertically integrated, and the positions along the section where the flow changes sign (positive to negative) was noted. This separates the section into negative and positive portions. The portion that was the smallest (i.e. most negative) and largest (i.e. most positive) were considered to be the Agulhas Current, and the Agulhas Return Current respectively. The boundaries of these positive and negative portions are considered the initial boundaries of the Agulhas Current and Agulhas Return Current as the north faces still need to be included. The north faces are only included if they have they meet two criteria: fall adjacent to the either the negative or positive portion, and attributed to the portion if they are the correct sign. This is performed along the section and determines the final boundaries of the Agulhas Current and Agulhas Return Current through the Crossroads section. These positions were then troubleshooted to ensure they correctly captured the two currents.

3.3.3.2 Troubleshooting

The first test plotted the four positions (ACstart, ACend, ARCstart and ARCstop) as a time series. The positions had to be in the correct order (ACstart $<$ ACend $<$ ARCstart $<$ ARCstop), and if they overlapped were further investigated (fig. 3.1).

To further investigate the incorrect positions, the surface and section velocity with the four positions were plotted to determine the dynamics causing the error (fig. 3.1). Two common problems were identified: the most negative portion (therefore the Agulhas Current) being too far offshore, and the ARCstop boundary including an eddy on the Agulhas Plateau. Two limitations were then applied to select the correct portion of the Agulhas Current, and the ARCstop boundary.

To ensure the correct portion was selected for the Agulhas Current position, all the negative portions over a certain value (i.e. too far offshore) are excluded, the most negative portion that is closest to the start of the section (i.e. the coast) is chosen. To stop the eddy on the Agulhas Plateau from being included by the ARCstop boundary, a value is used to limit the end point instead of a change in sign. This value was determined

by averaging the depth integrated velocities over the reanalysis products time period, which is assumed to be a reasonable approximation for the value.

3.3.3.3 limitations

The boundaries of the Agulhas Current and Agulhas Return Current are determined with the two limitations and are checked by the two methods described above. Incorrect boundaries are still identified, with no clear solution to correct the method, and these points have to be omitted.

Three events caused the above method to fail: early retroflection (Figure 3.1 - top row), ring shedding event (Figure 3.1 - middle row), and the Agulhas Plateau eddy (Figure 3.1 - bottom row). The correct boundaries could not be chosen in the early retroflection, and the ring shedding event because the Agulhas Current, and Agulhas Return Current do not flow through the Crossroads section. The method could not take it into account the influence of Agulhas Plateau eddy and the correct boundaries could not be selected.

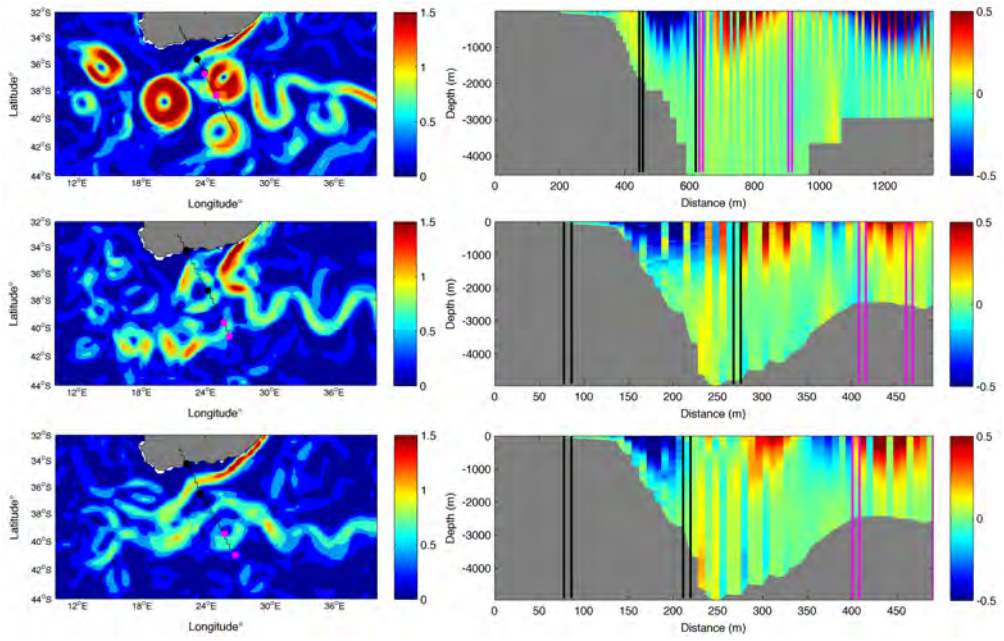

FIGURE 3.1: Typical boundary identification errors for the Agulhas Current and Agulhas Return Current over the Crossroads section due to a (top row) early retroflection, a (middle row) ring shedding event, and (bottom row) Agulhas Plateau eddy. The black dots and lines represent the boundaries of the Agulhas Current with the dot/line onshore representing ACstart, and offshore representing ACstop. The magenta dots and lines represent the boundaries of the Agulhas Return Current with the dot/line onshore representing ARCstart, and offshore representing ARCstop

From the determined boundaries we calculated the volume transport of the of the Agulhas Current and the Agulhas Return Current. Two types of volume transport are

calculated, the 'total' and 'jet' transport. The two different transports are calculated due to the possibly of alternating signs from the north/west faces in the section. This could artificially reduce the "total" transport.

The "total" transport is calculated using the specified boundaries determined above, and all the full depth velocities between these boundaries. The "jet" transport only uses the negative velocity values within the Agulhas Current boundaries, and the positive velocity values in the Agulhas Return Current boundaries. The Western Transport is calculated by the difference between the Agulhas Current transport and the Agulhas Return Current transport. Lastly, the mean and standard deviation is calculated for both the "total" and "jet" transport for the reanalysis products over the Crossroads section.

Chapter 4

Results

The results from the methods described above, are shown and described below. The results will be discussed further and related to the objectives of this thesis in Chapter 5.

4.1 Surface Validation

4.1.1 Velocity

The mean surface velocity is a good initial metric that shows the basic salient oceanographic features of the greater Agulhas Current System for MyOcean, HYCOM and Bluelink. In line with the objectives of this thesis, the mean surface velocity is validated against current literature and independent observations (ASAR), while revealing any initial structural problems. These initial structural problems, and the ability of data assimilation to constrain the numerical models in the reanalysis products will be investigated.

(A) MyOcean

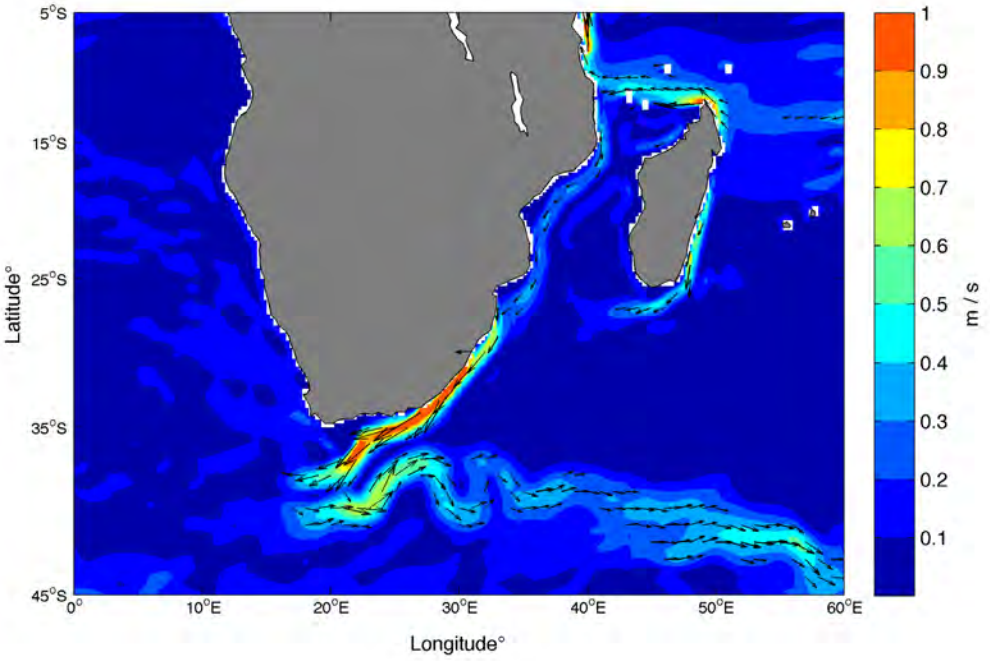

(B) HYCOM

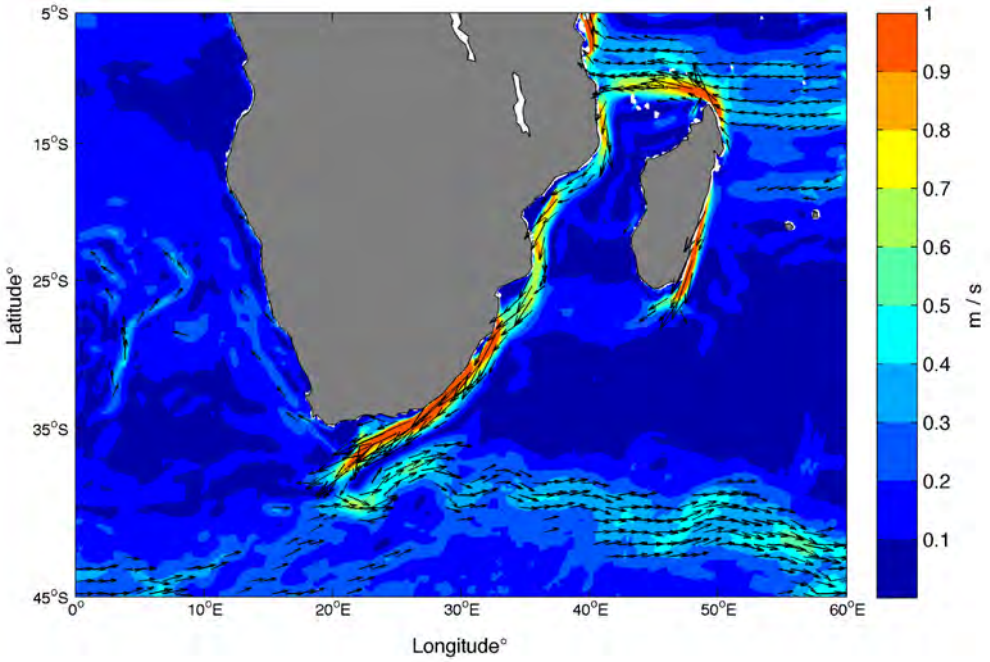

(c) Bluelink

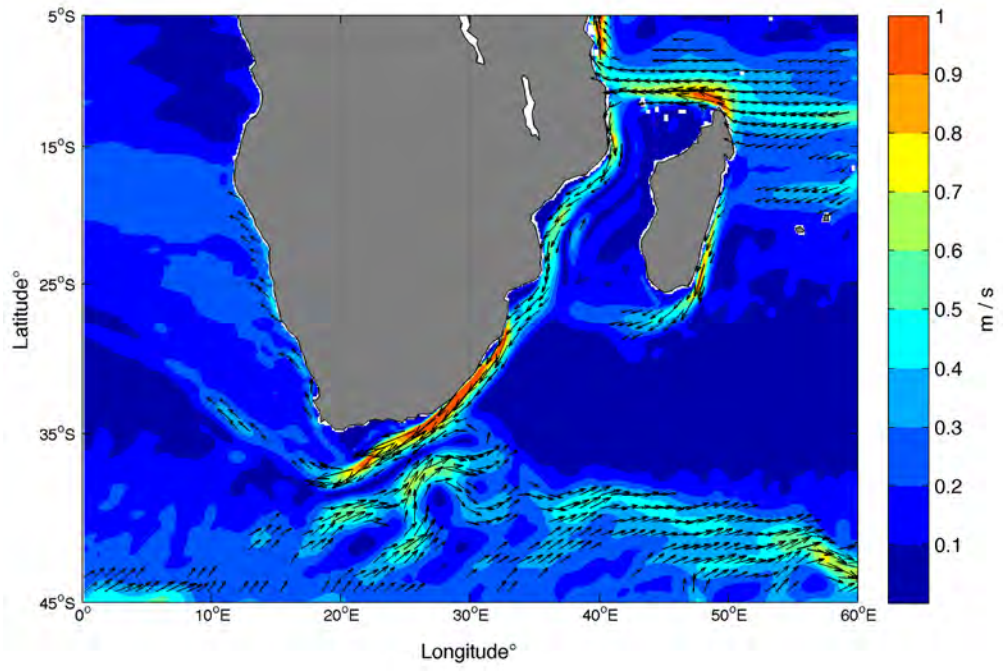

FIGURE 4.1: Mean sea surface velocity (m/s) of (a) MyOcean for 1993 to 2009, (b) HYCOM for 1993 to 2010, and (c) Bluelink for 2000 to 2010. The colour shading represents magnitude and the arrows show direction.

The mean surface velocity structure of MyOcean (fig. 4.1a) reproduces the basic salient oceanographic features within the greater Agulhas Current System. The South Equatorial Current (50°E, 10°S), East Madagascar Current (48°E, 10°S), Agulhas Current (26°S), and the Agulhas Return Current (40°S) are reasonably well represented in MyOcean.

The mean surface velocity structure in HYCOM (fig. 4.1b) is similar to MyOcean, showing the basic salient oceanographic features and currents of the greater Agulhas Current System. However HYCOM has a higher intensity compared to MyOcean in: the South Equatorial Current, the East Madagascar Current, and the Agulhas Current where large areas have velocities that are significantly larger than 1 m/s.

The mean surface velocity structure of Bluelink (fig. 4.1c) is comparable to MyOcean and HYCOM with a few exceptions. The South Equatorial Current (50°E, 10°S) is wider and stronger compared to MyOcean and HYCOM. The Agulhas Return Current, east of 35°E, is wider than both MyOcean and HYCOM. The velocity structure of the retroflection region in Bluelink compares poorly to MyOcean and HYCOM, and will need to be further investigated.

A flow through the western side of the Mozambique Channel (35°E, 20°S) is observed in all three reanalysis products. However this is an artifact of averaging the surface

velocities associated with the eddies propagating along similar paths through the channel and does not indicate there is a Mozambique Channel Current as discussed in Lutjeharms (2006).

The overall comparison between ASAR, and the reanalysis products (fig. 4.2) show that the structure of the Agulhas Current (particularly shape, and width) is well captured by all three reanalysis products. The main difference between the simulations and ASAR is the magnitude of the surface velocities.

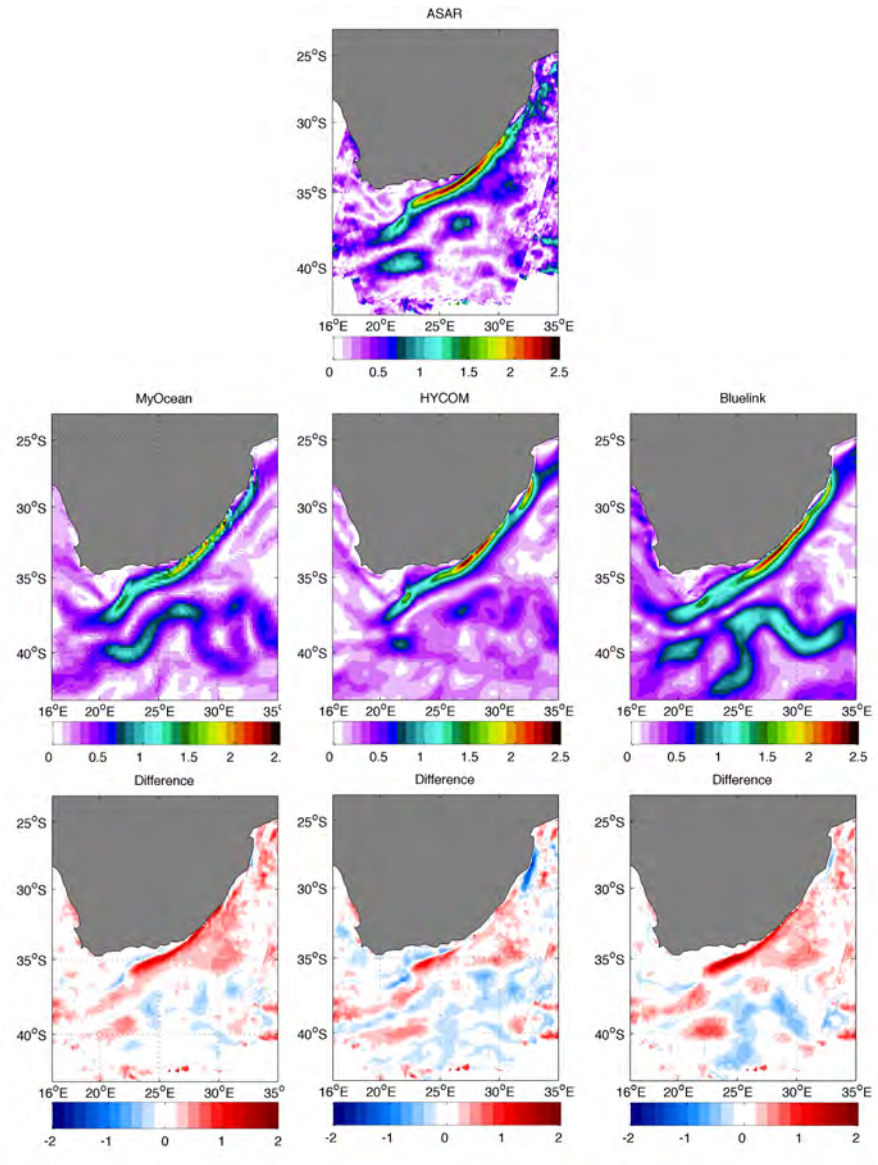

FIGURE 4.2: Comparison of mean surface velocity of ASAR (top row), MyOcean, HYCOM and Bluelink (middle row). The difference (ASAR - Model) (bottom row). The mean surface velocities are all averaged over 2008 to 2009. Red shading represents underestimation of the reanalysis product, while blue shading shows overestimation

MyOcean underestimates the overall Agulhas Current (25°E, 35°S) surface velocities by

approx. 1.5 m/s. HYCOM underestimates the southern Agulhas (23°E, 36°S) surface velocities by approx. 1.5 m/s, and overestimates the northern Agulhas (33°E, 23°S) by approx. 1.2 m/s. Bluelink underestimates the Agulhas Current (25°E, 35°S) surface velocities by approx. 2 m/s, and overestimates the Agulhas Return Current (25°E, 40°S) by approx. 1m/s, unlike MyOcean or HYCOM.

4.1.2 Barotropic streamfunction

The mean barotropic streamfunction (BTSF) shows the vertically integrated circulation of each reanalysis product (fig. 4.3). The mean BTSF shows the overall depth structure, the direction of flow and the integrated volume transport of MyOcean, HYCOM and Bluelink, which are important characteristics to be considered in the greater Agulhas Current System.

(A) MyOcean

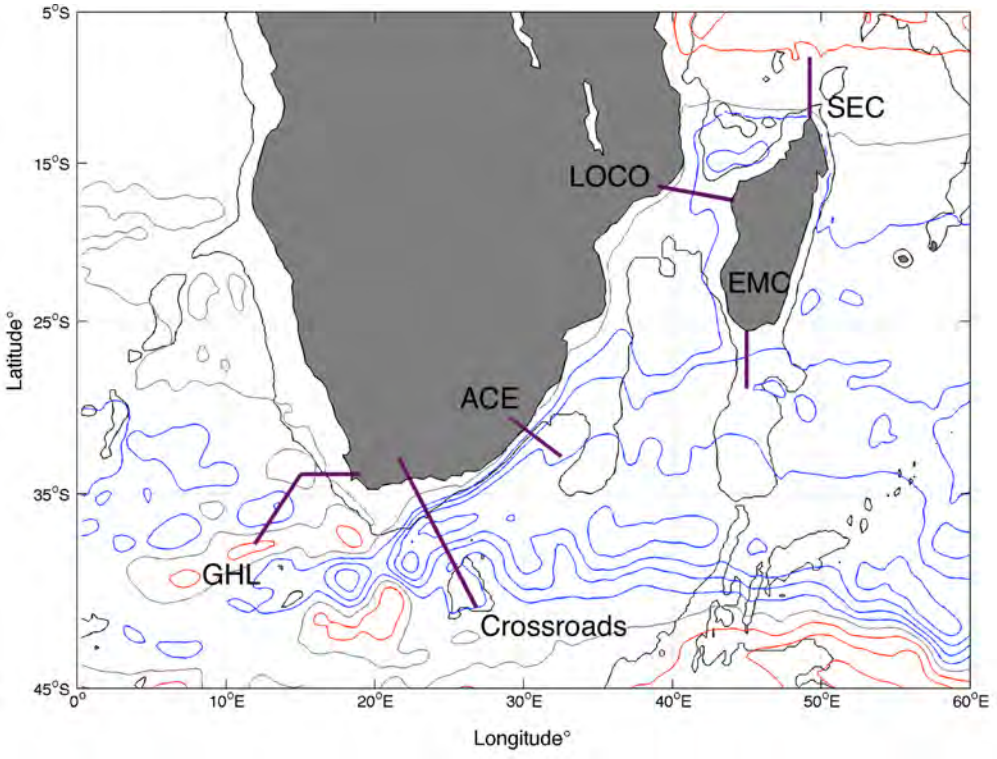

(b) HYCOM

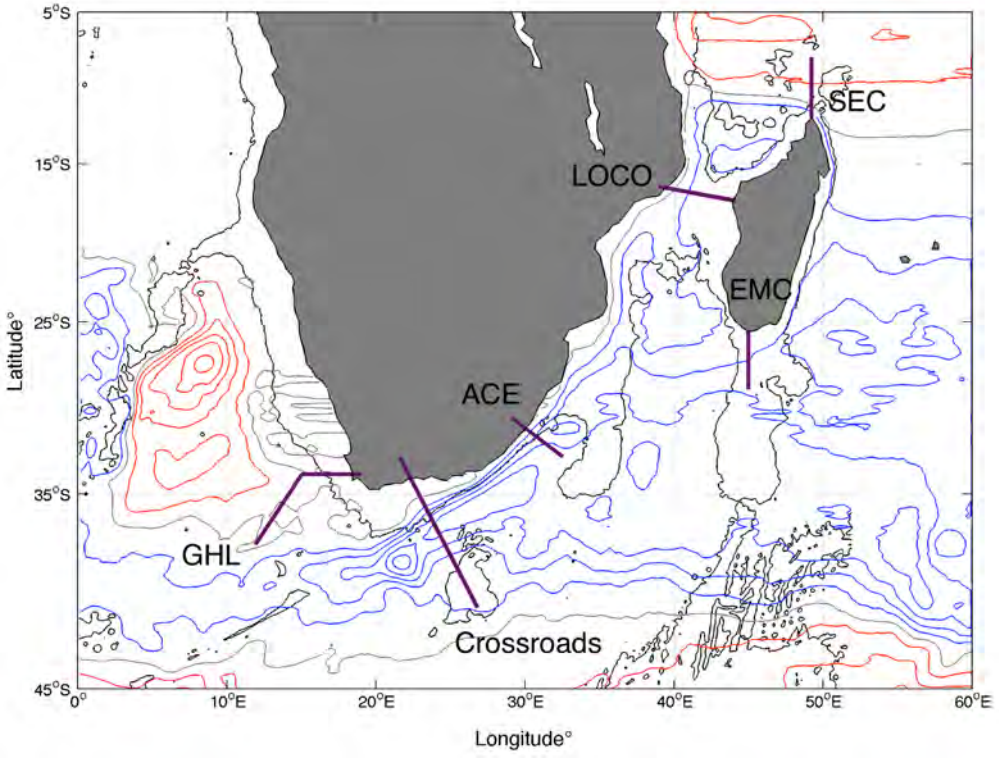

(c) Bluelink

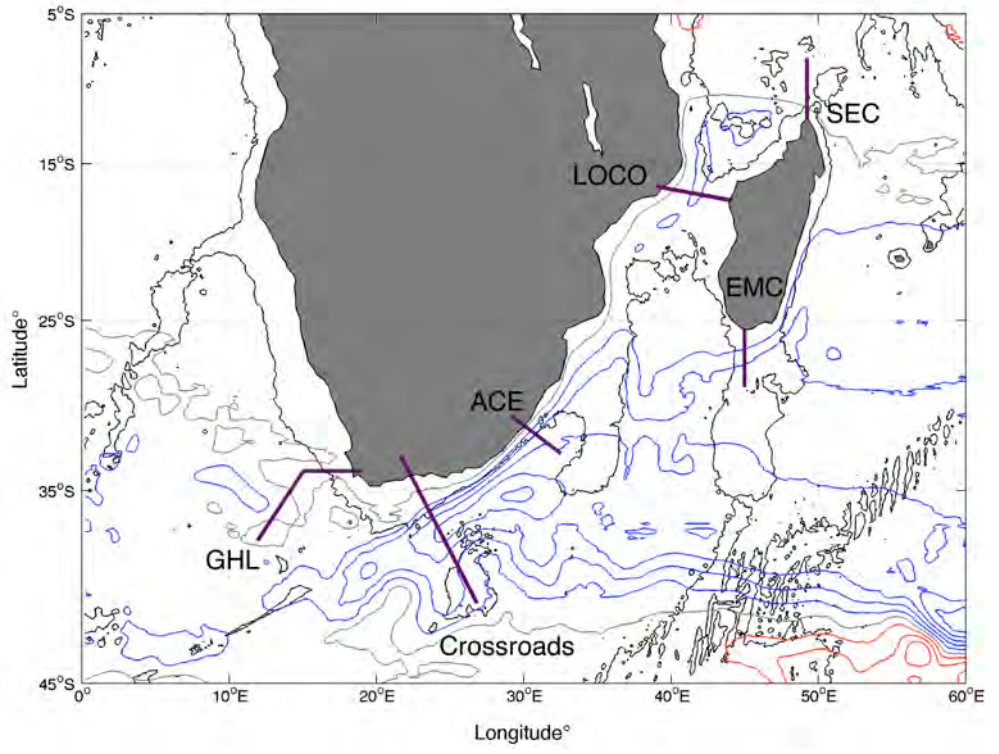

FIGURE 4.3: Mean barotropic streamfunction of (a) MyOcean for 1993 to 2009, (b) HYCOM for 1993 to 2010, and (c) Bluelink for 2000 to 2010. Contour interval of 20 Sv, with negative values shown in blue (anti-clockwise circulation), positive values in red (clockwise circulation), and zero contour in grey. Each respective reanalysis product's 3000 m isobath is shown in black

The overall circulation pattern in the BTSF of MyOcean (fig. 4.3a) is in good agreement compared to literature. The northern arm of the South Equatorial Current flows around the northern tip of Madagascar, and into the northern Mozambique Channel. This continues southward through the Mozambique Channel transporting 20 Sv, but an anticyclonic flow of 20 Sv remains north of the LOCO section. The southern arm of the South Equatorial Current flows south of Madagascar (27°S) through the EMC section transporting 20 Sv towards the Agulhas Current. These two flows with the addition of the recirculation (33°S) of the Agulhas Return Current contributes towards the total volume transport of the Agulhas Current.

The Agulhas Current simulated by MyOcean follows the continental shelf with a volume transport of 60 Sv, until it reaches the retroflection region (20°E, 37°S). At the Agulhas retroflection region the current turns upon itself towards the east becoming the Agulhas Return Current. The Agulhas Return Current meanders northward around the Agulhas Plateau (25°E, 40°S), stabilizing as it flows toward the South Indian Ocean. The eddy corridor from the retroflection region is represented by anti-cyclonic and cyclonic circulations of 20 Sv, observed in a northwestward direction from the retroflection position (22°E, 39°S).

The circulation pattern of HYCOM (fig. 4.3b) is similar to MyOcean with a few subtle differences. The source regions, the South Equatorial Current, the flow through the Mozambique Channel, and recirculation of the Agulhas Return Current have a similar circulation structure to MyOcean. Once again an anti-cyclonic circulation (44°E, 15°S) is present north of the LOCO line. The Agulhas Current, retroflection region, and the Agulhas Return Current also have a similar circulation pattern to MyOcean. The main difference in the circulation pattern in HYCOM is the eddy corridor from the retroflection region. An anti-cyclonic flow of 40 Sv travels directly west of the retroflection region, presumably the eddy corridor into the South Atlantic. Another significant difference is a large positive anomaly of 100 Sv that lies off the west coast of South Africa.

The circulation pattern of Bluelink (fig. 4.3c) differs significantly compared to MyOcean (fig. 4.3a) and HYCOM (fig. 4.3b). The South Equatorial Current flows westward until it reaches Madagascar, and flows southward along the east coast through the EMC section transporting 40 Sv toward the Agulhas Current. Through the SEC and LOCO sections there is no observed flow greater than 20 Sv. Once again north of the LOCO section (45°E, 13°S) lies an anticyclonic flow of 20 Sv. The flow through the EMC section is larger, 40 Sv compared to 20 Sv, in MyOcean and HYCOM, and there is no evidence of recirculation of the Agulhas Return Current. The Agulhas Current flows southwestward following the continental shelf until the retroflection region (25°E, 37°S). At the retroflection region, the flow turns back on itself meandering over the Agulhas

Plateau (27°E, 40°S), becoming the Agulhas Return Current (40°S), continuing eastward until it reaches the South Indian Ocean. The position of the retroflection region is further northeastward compared to MyOcean, and HYCOM. The eddy corridor is represented by anti-cyclonic flow west and northwestward of the retroflection region.

4.1.3 Surface variability

The mean sea surface height (SSH), and standard deviation of SSH (proxy for mesoscale variability) shows the mean position and mesoscale variability of the Agulhas Current System respectively. These are essential metrics to include as the Agulhas Current has high levels of mesoscale variability, and common problems occur in simulating the correct position of the Agulhas Current retroflection region (Penven et al., 2011). The mean SSH and SSH standard deviation are plotted for MyOcean, HYCOM, Bluelink, and AVISO (fig. 4.4). The contours of mean SSH and SSH standard deviation are validated against current literature. AVISO is used to investigate the ability of data assimilation to constrain the numerical models as the contours of mean SSH and SSH standard deviations differ vastly between the three reanalysis products.

(A) MyOcean

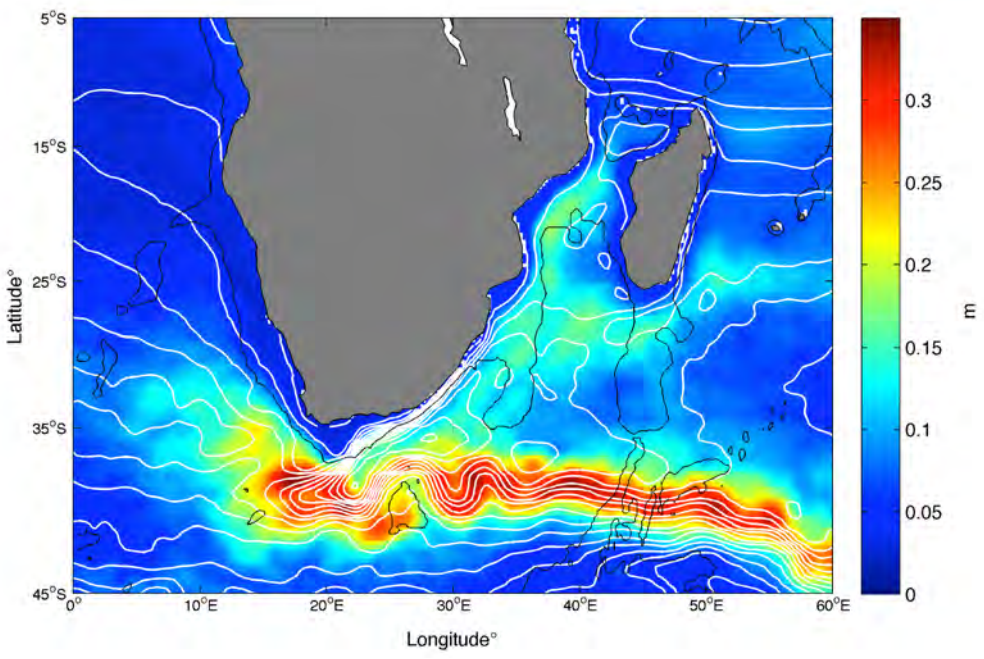

(B) HYCOM

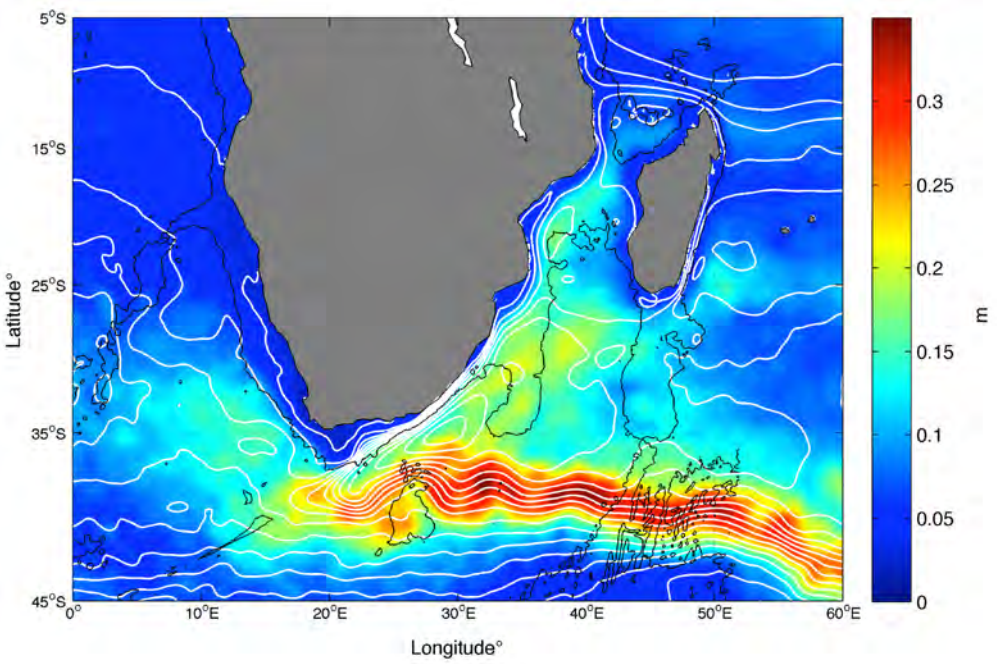

(C) Bluelink

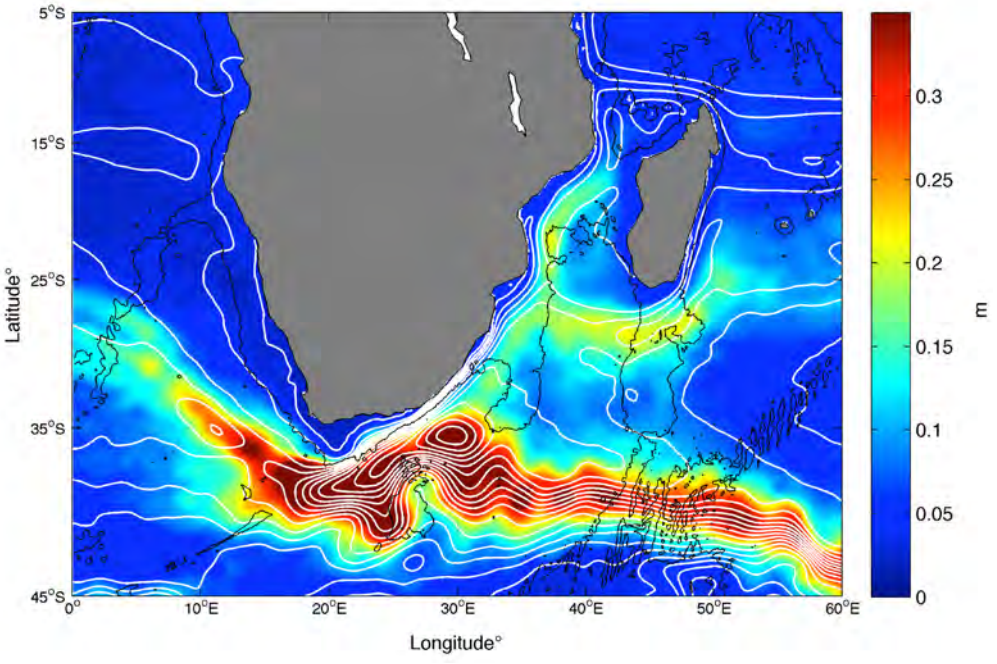

(d) AVISO

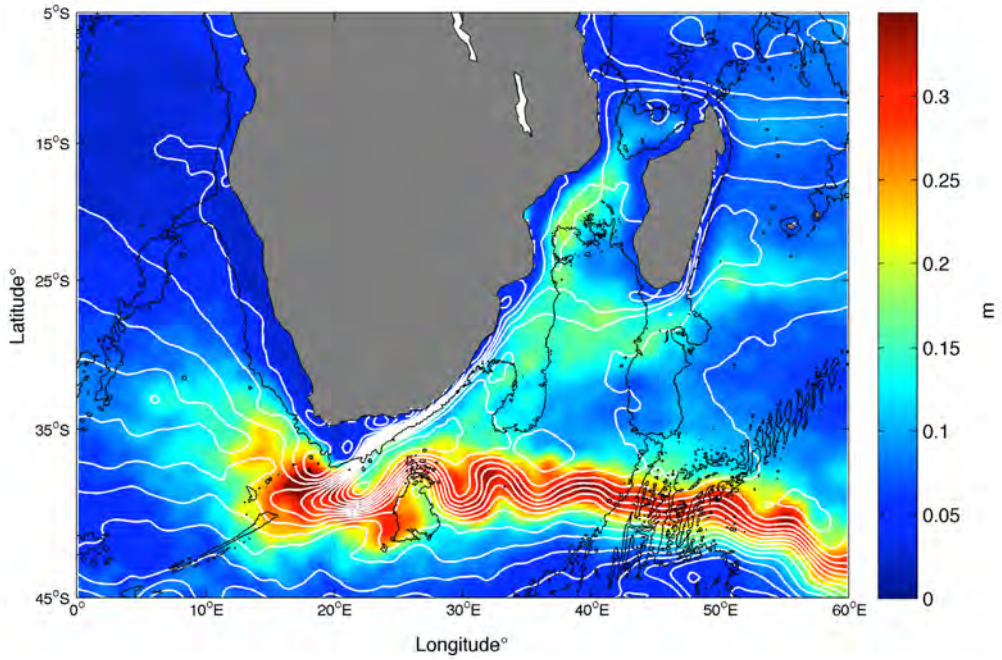

FIGURE 4.4: Mean SSH is represented by white contours and the mean surface SSH standard deviation represented by the colour shading is shown for (a) MyOcean for 1993 - 2009, (b) HYCOM for 1993 - 2010, (c) Bluelink for 2000 - 2010, (d) AVISO for 1993 - 2010. Each respective reanalysis product's 3000 m isobath is shown in black, and ETOPO 2v2 is used for AVISO.

The contours of mean SSH clearly shows the Agulhas Current (32°E, 30°S), the retroflection region (22°E, 39°S) and the Agulhas Return Current (40°E, 40°S). The contours of mean SSH in both MyOcean and HYCOM shows the Agulhas Current flowing along the continental shelf closely until it leaves the Agulhas Bank (20°E, 36°S), retroflecting, and becoming the Agulhas Return Current. The Agulhas Return Current meanders northward around the Agulhas Plateau (26°E, 40°S), and continues eastward with the meanders being reduces as it flows towards the South Indian Ocean.

The contours of mean SSH in Bluelink is does not compare favorably to the other two simulations having a vastly different structure in the Agulhas Current, retroflection region, and the Agulhas Return Current. The Agulhas Current flows southwestward following the continental shelf until it retroflects to become the Agulhas Return Current. However the structure of the retroflection region is incorrect, displaying an extra meander (24°E, 42°S). The Agulhas Return Current meanders over the Agulhas Plateau and too far north. After the Agulhas Plateau, the Agulhas Return Current has a major meander moving the position of the current south. The Agulhas Return Current then continues to flow eastward with minimal meanders or perturbations.

The mean SSH standard deviation is significantly different between MyOcean, HYCOM and Bluelink (fig. 4.4). Four common areas of high SSH standard deviation can be observed: the Mozambique Channel (40°E, 20°S), south of Madagascar (45°E, 27°S), the retroflection region (20°E, 40°S), and the Agulhas Return Current (35°E, 40°S).

In MyOcean, the Agulhas Return Current and the retroflection region have the highest values (0.35 m), the Mozambique Channel having an intermediate value (0.175 m), and south of Madagascar having the lowest (0.125 m). The SSH standard deviation in the retroflection region also expands in a northwestward direction into the South Atlantic depicting the eddy pathways. Over the Agulhas Plateau (27°E, 40°S) there is a large value of mean SSH standard deviation (0.175 m).

HYCOM has a notably different SSH standard deviation structure to MyOcean, with an overall higher SSH standard deviation over the greater Agulhas Region. Similarly to MyOcean, HYCOM has areas of high SSH standard deviation: the Mozambique Channel (40°E, 20°S) of 0.175 m, south of Madagascar (45°E, 27°S) of 0.125 m, the retroflection region (20°E, 40°S) of 0.2 m, and the Agulhas Return Current (35°E, 40°S) of 0.35 m. Over the Agulhas Plateau (27°E, 40°S), an intermediate valued of SSH standard deviation can be observed. A wide pathway of SSH standard deviation (0.15 m) expands from the retroflection region into the South Atlantic.

Bluelink unlike MyOcean and HYCOM, has a drastically different mean SSH standard deviation pattern. The four main regions of SSH standard deviation are also shown in Bluelink: the Mozambique channel (40°E, 20°S) of 0.175 m, south of Madagascar (45°E, 27°S) of 0.2 m, the retroflection region (20°E, 40°S) greater than 0.35 m, and the Agulhas Return Current (35°E, 40°S) greater than 0.35 m.

The SSH standard deviation pattern over the retroflection region, Agulhas Return Current and pathway into the Atlantic, are significantly different compared to MyOcean and HYCOM. A high, narrow and focused pathway (0.3m) of SSH standard deviation expands into the South Atlantic. The Agulhas Plateau (27°E, 40°S) is mainly covered by a high SSH standard deviation, but varies in intensity over the eastern and western sides (0.35 to 0.15 m).

The SSH standard deviation from AVISO shows the four common areas to the three reanalysis products. The Mozambique Channel (0.175 m), south of Madagascar (0.15 m), the retroflection region (0.35 m), and the Agulhas Return Current (0.30 m). The SSH standard deviation expands as a wide pathway (0.175 m) from the retroflection region in a north-westward direction into the South Atlantic. Over the Agulhas Plateau (27°E, 40°S) the mean SSH standard deviation varies between 0.15 to 0.35 m.

4.2 Section Validation

To validate the volume transport and velocity over the greater Agulhas Current System, six sections of volume transport and velocity are extracted from key locations within the greater Agulhas Current systems (fig. 3.1). The transport values from these six sections for MyOcean, HYCOM and Bluelink are first investigated by comparing the reanalysis products to current literature (Table 4.1). The transport at LOCO is further investigated by validating the reanalysis products against results from an *in-situ* mooring study. The transport and velocity at ACE is further validated by comparing the reanalysis products against *in-situ* mooring data. The constraining of the numerical model by data assimilation is investigated only at ACE and LOCO.

4.2.1 Volume transport

4.2.1.1 Overview

Section	MyOcean	HYCOM	Bluelink	Observations
SEC	-42.83 ± 12.42	-50.32 ± 10.94	-34.05 ± 7.96	-26.90 ± 9.40
EMC	-22.35 ± 16.18	-35.86 ± 12.03	-36.45 ± 17.50	≈ -37.00
LOCO	-24.95 ± 7.90	-24.12 ± 7.00	-18.32 ± 6.01	-16.41 ± 9.84
ACE	-56.03 ± 20.90	-66.03 ± 24.11	-63.22 ± 22.91	-69.70 ± 4.30
Crossroads	-4.14 ± 17.47	-21.46 ± 24.00	-26.70 ± 31.85	N/A
GHL	100.01 ± 11.36	84.93 ± 14.44	70.45 ± 8.67	≈ 15.00

TABLE 4.1: Mean and standard deviation of volume transport (Sv) through six sections in the greater Agulhas Current system for MyOcean (1993 to 2009), HYCOM (1993 to 2010), Bluelink (2000 to 2010) and available observations

The mean volume transport through the SEC section of MyOcean and HYCOM are double the observed magnitude, while Bluelink overestimates the observed magnitude by approx. 10 Sv (Swallow et al., 1988). The standard deviation in MyOcean, HYCOM and Bluelink are all similar to the standard deviation estimated by the observations. The EMC section indicates that the mean volume transport of Bluelink is comparable to observations. However HYCOM, and Bluelink overestimate the mean volume transport by approx. - 8 Sv (Nauw et al., 2008).

The volume transport through the LOCO section can be accurately compared to the observations (Ridderinkhof et al., 2010). Both MyOcean and HYCOM overestimate the mean transport by approx. 8 Sv (± 60% of the total observed transport), while

Bluelink compares well with the mean observed transport. The standard deviation of transport through LOCO of the reanalysis products all have comparable values to the observations, suggesting the variability in the transport is well accounted for.

In the core of Agulhas Current, transport through the ACE section reveals that HYCOM, and Bluelink closely represent the mean transport compared to the observations, but MyOcean underestimates the mean transport by approx. 15 Sv. The standard deviation produced by the reanalysis products are all similar to each other (approx. 20 Sv), but considerably larger than the observed value (4 Sv) (Bryden et al., 2005).

The Crossroads section is a recently established transect to investigate the Agulhas Current and Return Current, of which the observational results are still in progress (Ansorge, 2014). HYCOM, MyOcean, and Bluelink have highly variable values for both mean and standard deviation. Finally the GHL section, which is commonly used to estimate the Agulhas Leakage has varied results between the different reanalysis products. MyOcean drastically overestimates (100 Sv), followed by HYCOM (85 Sv), and lastly Bluelink (70 Sv). These are significantly larger than the approx. 15 Sv estimated from observations (Richardson, 2007).

4.2.1.2 LOCO

The transport time series through the LOCO section for 2004 to 2009 (fig. 4.5), shows the ability of the reanalysis products to correctly simulate the volume transport through the Mozambique Channel. The time series indicates that the reanalysis products are not able to recreate the exact range of the observed transports (10 Sv to -40 Sv), but are still relatively comparable.

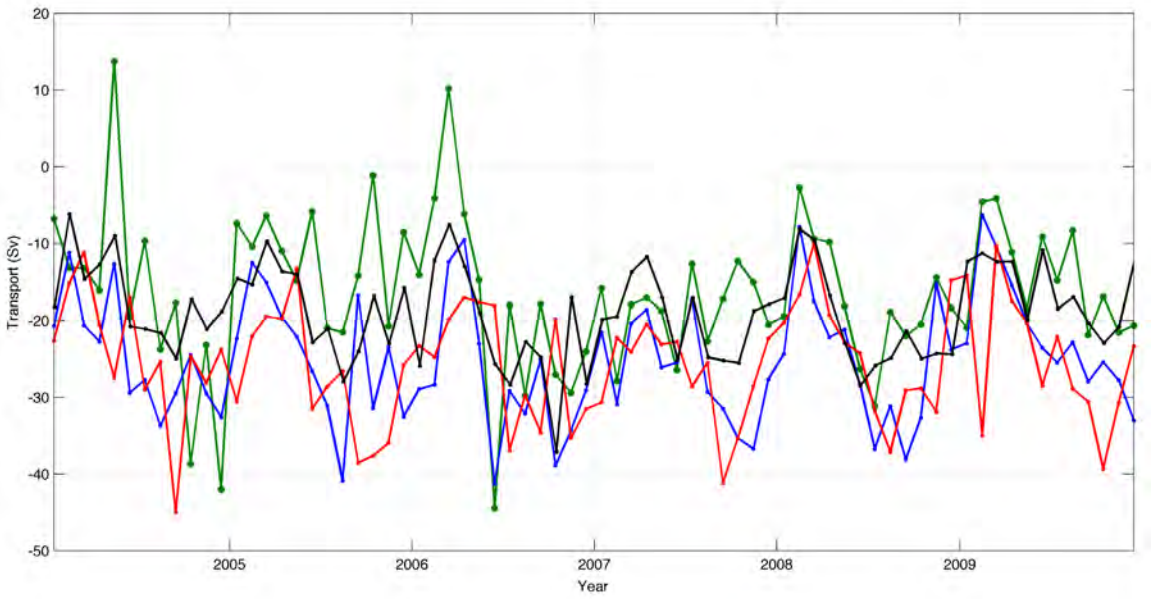

FIGURE 4.5: Transport (positive northwards) through the LOCO section of *in-situ* moorings (green), MyOcean (blue), HYCOM (red), and Bluelink (black) for January 2004 - December 2009

The mean values (Table 4.2) of MyOcean and HYCOM significantly overestimate the observed transport by approx. 10 Sv, while Bluelink is better. The mean transport in Bluelink is in relatively close agreement with the observed transport, while MyOcean and HYCOM significantly overestimate the mean.

	Observations	MyOcean	HYCOM	Bluelink
Mean	-16.41	-25.04	-25.57	-18.94
Standard Deviation	9.84	7.99	7.68	6.09
Correlation (Incl. Seasonality)		0.62	0.07	0.55
Significance level		95	90	95
Correlation (Excl. Seasonality)		0.48	0.17	0.33
Significance level		95	90	95

TABLE 4.2: Mean and standard deviation of the volume transport (positive northwards) through the LOCO section for January 2004 to December 2009. Correlation is calculated between each reanalysis product, and the *in-situ* moorings with the level of significance shown.

The standard deviation of all three reanalysis products have similar values of approx. 8 Sv, which is close to the observed value. This result suggests that the reanalysis products are capturing the same level of variability as in the observations, but not in the same range. The positive correlation between the observations and MyOcean (0.62), and Bluelink (0.55) with a significance level of 95% shows some agreement with

the observations. The lower correlation of 0.07 at 90% significance level for HYCOM indicates that it does not to reproduce the variability observations.

From the transport time series (fig. 4.5) a clear seasonal signal can be distinguished, from both the reanalysis products, and the observations. The influence of the seasonal signal was was further investigated using a power density spectrum (fig. 4.6).

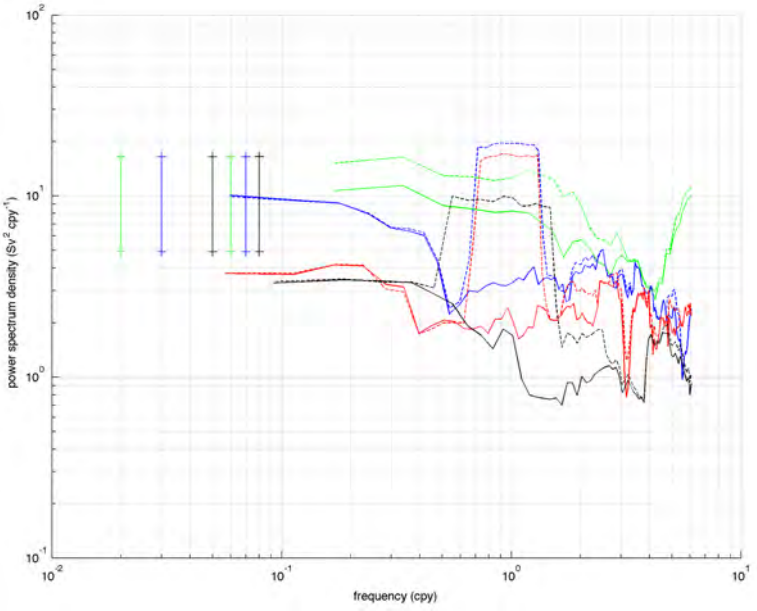

FIGURE 4.6: Power density spectrum of transport through the LOCO section of the *in-situ* moorings (green), MyOcean (blue), HYCOM (red), and Bluelink (black). Dashed lines include the seasonal cycle, while solid lines have removed the seasonal cycle. The frequency is shown in cycles per year.

The power density spectrum (fig. 4.6) of the LOCO transport time series clearly shows the frequency of the seasonal cycle. The dashed lines include the seasonal cycle, which show a large peak falling outside the error bar at the three month frequency. This confirms that there is a strong seasonal component in the transport time series of the reanalysis products, and the observation. The seasonal cycle is then removed to further investigate other signals (solid lines) and shows that across frequencies, the observations have the highest variance, followed by MyOcean, HYCOM, and Bluelink with the lowest. At the higher frequencies, MyOcean and HYCOM reproduce a similar level of variability compared to the observations. To further investigate the transport anomalies (excluding the seasonal cycle) and event scale features within the transport time series, the time series was plotted for 1993 to 2010.

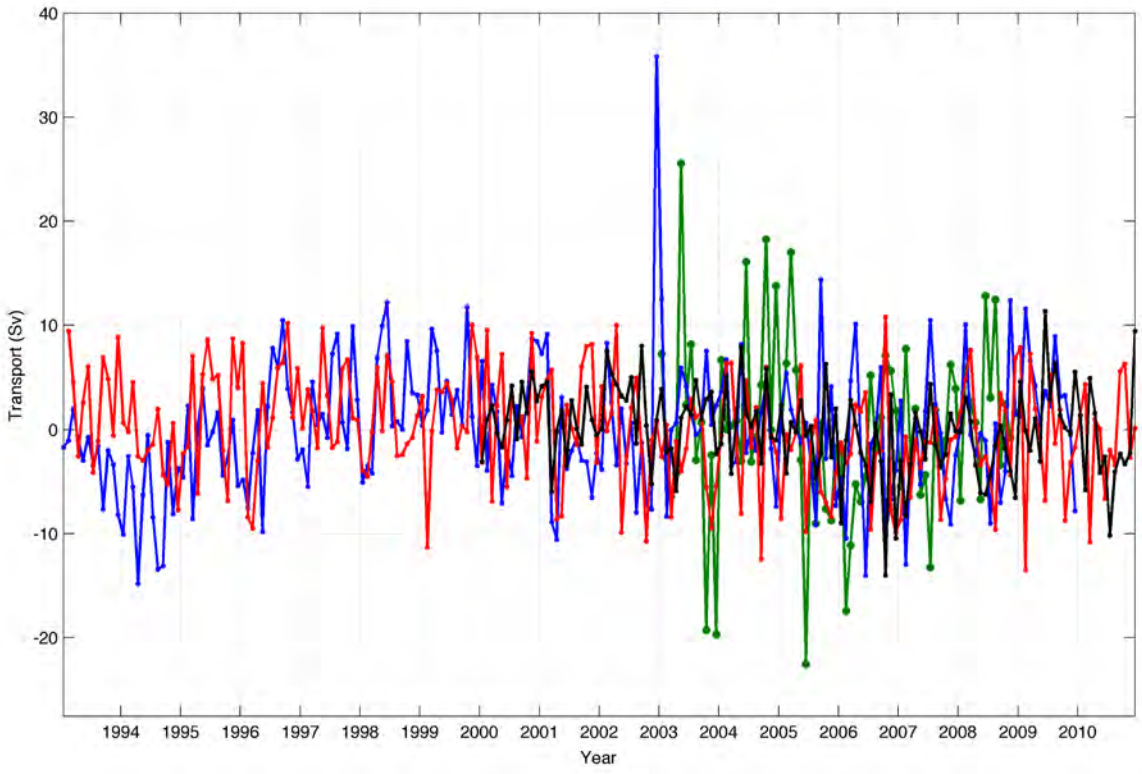

FIGURE 4.7: Volume transport anomalies (excluding seasonal cycle) through the LOCO section of *in-situ* moorings (green) for 2004 to 2009, MyOcean (blue) for 1993 to 2009, HYCOM (red) for 1993 to 2010, and Bluelink (black) for 1993 to 2010.

The transport anomalies (fig. 4.7) reveal differences in the event scale features and range between the reanalysis products and observations. This indicates that seasonality is the main signal responsible for the reasonable correlation between the reanalysis products and observations. The correlation values (Table 4.2) for MyOcean (0.62 to 0.48 at 95% significance level), and Bluelink (0.55 to 0.33 at 95% significance level) have decreased. However HYCOM (0.07 to 0.17 at 90% at significance level) has increased. The decrease in correlation of MyOcean, and Bluelink suggests that the transport time series produced by the reanalysis products cannot simulate the variability of the observed volume transport at the event scale, while the increase in correlation in HYCOM is insignificant.

4.2.1.3 ACE

The transport time series (fig. 4.8) through the ACE section can be used to validate the reanalysis products, as it has not been assimilated into the reanalysis products. Bluelink is not available over the time period of the observations and is omitted. The transport time series shows MyOcean has a lower mean value of 58 Sv (southward) compared to

the observations with 79 Sv (Table 4.3). However MyOcean has a similar range from -80 Sv to -20 Sv compared to the observations with -110 Sv to -50 Sv.

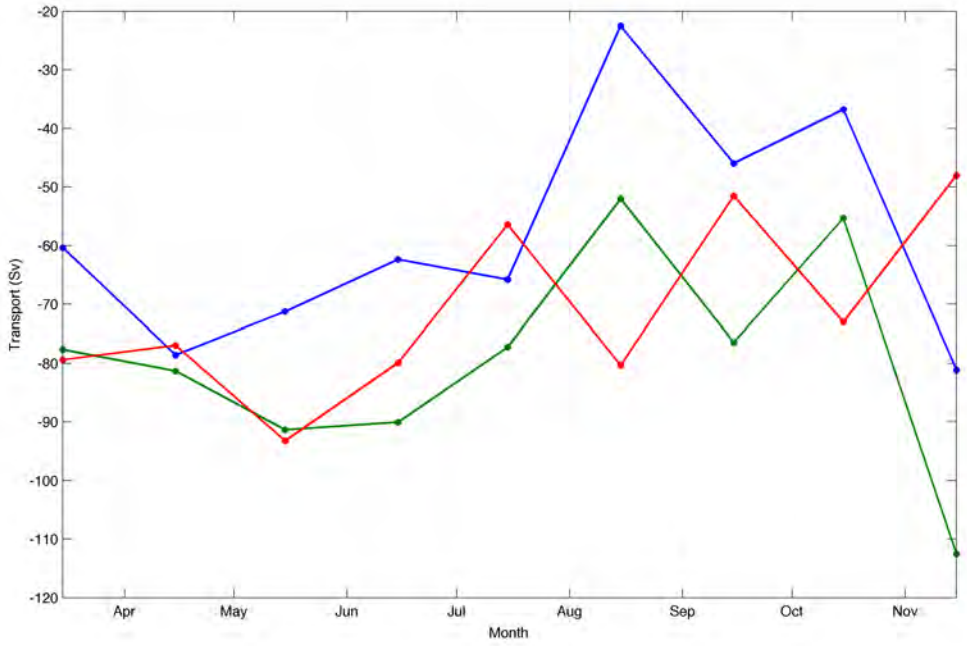

FIGURE 4.8: Volume transport through the 32°S section of *in-situ* moorings (green), MyOcean (blue), and HYCOM (red) for February 1995 to November 1995.

	Observations	MyOcean	HYCOM
Mean	-79.34	-58.32	-70.98
Standard Deviation	18.39	19.60	15.37
Correlation		0.87	0.27
Significance level		95	90

TABLE 4.3: Mean and standard deviation of volume transport through the 32°S line for the period 01 February 1995 to 24 November 1995. Correlation calculated between each reanalysis product, and the *in-situ* moorings with the accepted level of significance.

HYCOM has a comparable mean value of -70 Sv against the observations with -79 Sv (Table 4.3), but a smaller range of -90 to -40 Sv compared to the observations with a range of -110 Sv to -50 Sv. The standard deviation of MyOcean (19 Sv) and HYCOM (15 Sv) are in close agreement with the observations (18 Sv).

The event scale features are well represented in MyOcean and are closely correlated to the observations (0.87 at 95% significance level), while HYCOM did not reproduce the event scale features and is poorly correlated to the observations (0.27 at 90% significance

level). To further investigate the event scale features and range, the transport time series is investigated between 1993 to 2010, with each reanalysis product and observation being plotted on their full respective time period.

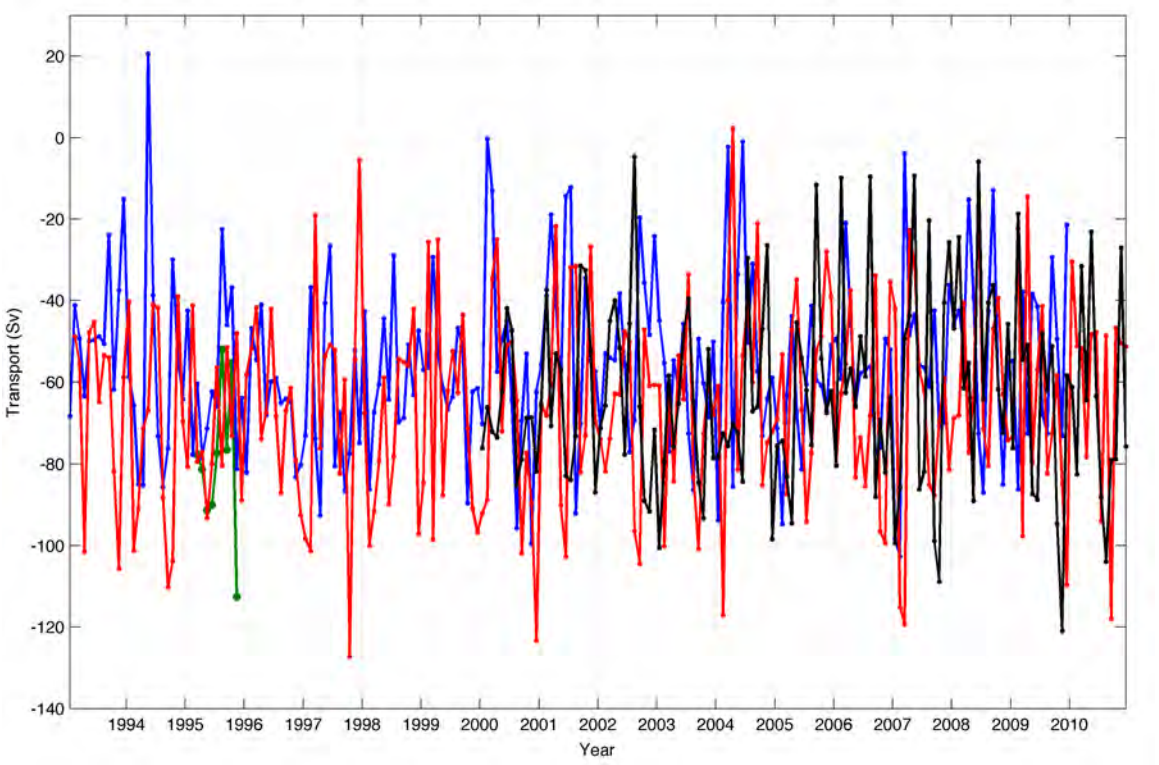

FIGURE 4.9: Volume transport through the 32°S section of *in-situ* moorings (green) for 1995, MyOcean (blue) for 1993 to 2009, HYCOM (red) for 1993 to 2010, and Bluelink (black) for 1993 to 2010.

Though these simulations cannot be directly validate against observations, it is important to note the differences in the mean, standard deviation, range, and event scale features between MyOcean, HYCOM and Bluelink. The mean transport values of HYCOM, and Bluelink, are comparable (approx. -65 Sv), while MyOcean is smaller (-55 Sv). The standard deviation across MyOcean, HYCOM, and Bluelink all have a similar value approx. 24 Sv indicating they all represent the variability in the transport time series well. No clear signal or common range can be seen from fig. 4.9, and event scale features diverge between the reanalysis products.

4.2.1.4 Crossroads

Over the Crossroads section, the Agulhas Current, and the Agulhas Return Current have been differentiated (see chapter 3), which enables the calculation of volume transport that leaves the Agulhas Current System (i.e. Westward Transport)(Table 4.4). Due to

the lack of data at depth in HYCOM, we were unable to calculate the jet transport through the Crossroads section.

		MyOcean		HYCOM		Bluelink	
		Total	Jet	Total	Jet	Total	Jet
AC	Mean	-93	-101	-85	N/A	-94	-105
	Standard deviation	14	14	21	N/A	33	31
ARC	Mean	82	95	73	N/A	68	83
	Standard deviation	28	22	25	N/A	35	34
WT	Mean	-11	-6	-19	N/A	-25	-22
	Standard deviation	22	21	19	N/A	31	34

TABLE 4.4: Mean and standard deviation of volume transport of the Agulhas Current (AC), the Agulhas Return Current (ARC), and the Westward Transport (WT) through the Crossroads section. Refer to chapter 3 for definition of total and jet transport

The total mean transport of the Agulhas Current is in good agreement between MyOcean (-93 Sv), HYCOM (-85 Sv), and Bluelink (-94 Sv), while the mean jet transport is comparable between MyOcean (-101 Sv) and Bluelink (-105 Sv). The standard deviation of both total, and jet transport is highest in Bluelink (30 Sv), followed by HYCOM (20 Sv), and finally MyOcean (14 Sv) with the smallest.

The Agulhas Return Current has comparable mean values across the reanalysis products. MyOcean shows similar transport values between the total (82 Sv), and jet (95 Sv) transports. HYCOM has a mean total transport value (95 Sv) over the Agulhas Return Current. Bluelink has a significant difference between the total (68 Sv), and jet (83 Sv) transport. The standard deviation over the Agulhas Return Current is highest in Bluelink (approx. 35 Sv), followed by MyOcean (approx. 26 Sv), with HYCOM (11 Sv) having the lowest.

The mean Westward Transport in MyOcean (-11 Sv), HYCOM (-19 Sv) and Bluelink (-25 Sv) are of similar magnitude to estimates of Agulhas Leakage (approx. -18 Sv) in Richardson (2007). MyOcean has a significant difference (5 Sv) between the total (-11 Sv) and jet (-6 Sv) transports, while Bluelink shows a small difference (-3 Sv) between the total (-25 Sv) and jet (-22 Sv) transport.

4.2.2 Velocity

4.2.2.1 ACE

The mean velocity sections at ACE facilitate a basic comparison of the vertical velocity structure of the reanalysis products and observations (fig. 4.10). Unfortunately only MyOcean can be compared directly to the observations as Bluelink (2000 to 2010) does not cover the same observational time period (February to March 1995), and at the time of writing the depth velocity in HYCOM as previously discussed is incorrect.

(A) MyOcean

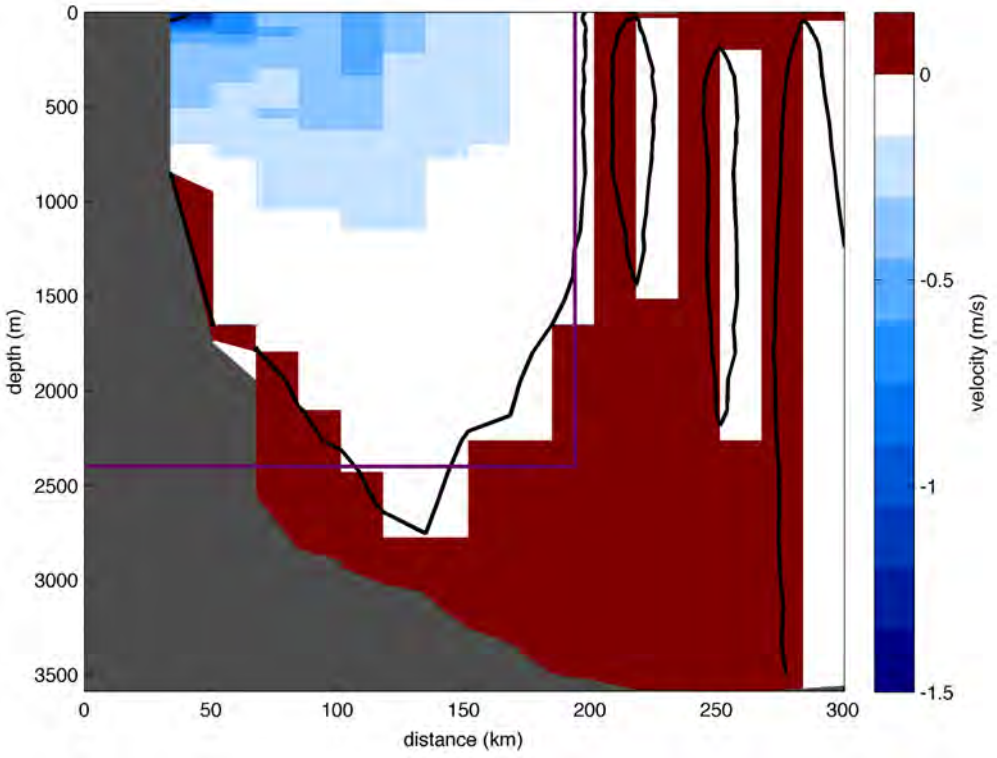

(b) Bluelink

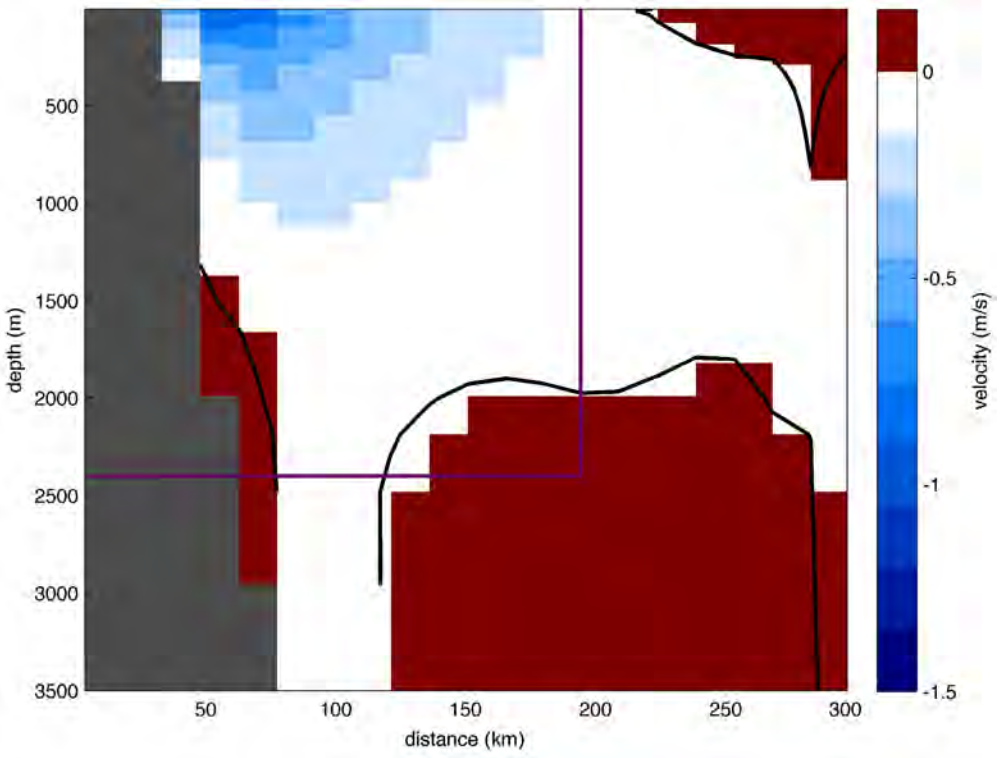

(c) ACE 32°S

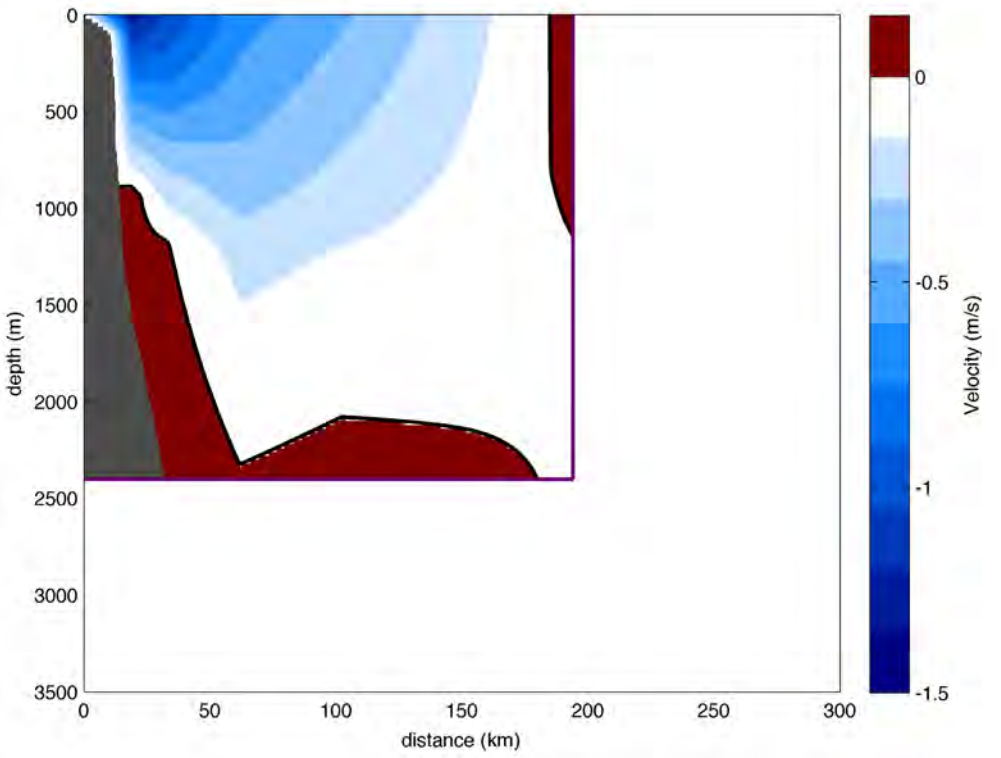

FIGURE 4.10: Mean velocity section at 32°S for MyOcean (a) for February 1995 to November 1995, Bluelink (b) for 2000 to 2010, and the *in-situ* moorings (c) from February 1995 to November 1995. Zero isotach is contoured, and the purple block outlines the observational area

MyOcean has a narrower, concentrated, but overall weaker Agulhas Current, while the observations show a dissipated, wide, and strong current. The location of the undercurrent is accurately represented by MyOcean, but underestimates the velocity. Although the mean period in Bluelink is different from the observations, the key features of the Agulhas Current can be observed. The velocity is correctly dissipated throughout the whole section, and a wide current and clear undercurrent in the correct location is evident

Chapter 5

Discussion

The validation of the global reanalysis products to accurately represent the Agulhas Current system is an important step in developing a dedicated regional prediction system. In this study, the products from three global prediction systems were validated against the Agulhas Current literature and unassimilated observations. Through the validation process of MyOcean and HYCOM the ability of data assimilation to constrain the numerical models was investigated. Here we discuss the results shown in chapter 4.

5.1 Surface structure and variability

5.1.1 Velocity

The mean surface velocities (fig. 4.1) of MyOcean, HYCOM and Bluelink shows a circulation pattern that is in good agreement compared to current literature (Lutjeharms, 2006; Ansorge and Lutjeharms, 2007). The salient oceanographic features clearly shown in the Agulhas System are the: South Equatorial Current, East Madagascar Current, South East Madagascar, Agulhas Current, position of the retroflection region, eddy corridor, and Agulhas Return Current. However the structure of the retroflection region in Bluelink is poorly represented compared to MyOcean, HYCOM and documented literature (Lutjeharms, 2006), and requires further investigation.

The mean surface velocity from the reanalysis products are validated by velocities derived from ASAR (fig. 4.2). The comparison with ASAR confirms the difficulty of MyOcean, HYCOM, and Bluelink to correctly reproduce the velocity magnitudes. However this is expected for MyOcean and HYCOM as the prediction systems assimilate altimetry sea level anomaly, which underestimates the velocities in the Agulhas Current

(Rouault et al., 2010). Combined with the inaccuracies of the numerical model, the velocity magnitudes diverge.

The structure of the Agulhas Current of MyOcean, HYCOM and Bluelink are comparable in the overall shape and width when compared to ASAR. The assimilated SSH in MyOcean and HYCOM will play a role in ensuring the correct structure of the Agulhas Current is simulated, and the we can observe the numerical model is somewhat constrained by the assimilated observations.

The circulation pattern in ASAR also reveals the affect of topographic steering of the southern Agulhas Current. The trajectory and shape of the main Agulhas Current as the continental shelf widens in MyOcean and HYCOM are comparable. However Bluelink is contradictory to MyOcean and HYCOM and poorly simulates the topographic steering. The poor simulation adjacent to the bathymetry will be discussed further in section 5.1.2.

5.1.2 Barotropic streamfunction

The BTSF (fig. 4.3) shows the full depth flow structure over the greater Agulhas Current System. The BTSF shows similar structures from the mean surface velocity (fig. 4.1) representing the major salient oceanographic features. However the BTSF reveals inaccuracies in the certain salient features in MyOcean, HYCOM and Bluelink.

All the reanalysis products generated a circular flow (20 Sv) north of the LOCO section, which is created due to the time averaging of anti-cyclonic eddies in the Comoras Basin (Collins et al., 2014). The presence of the anti-cyclonic eddy north of the LOCO section shown in the reanalysis products is most probably due to the assimilated data (SSH) compared to the numerical model. Collins et al. (2014) shows a large number of anti-cyclonic eddies from the AVISO dataset that will heavily influence our reanalysis products.

The structure of BTSF surrounding Madagascar in MyOcean and HYCOM is comparable, while in Bluelink shows a different flow structure. The BTSF in MyOcean and HYCOM shows a clear flow of the South Equatorial Current, around the northern and southern tips of Madagascar, through the Mozambique channel and finally into the Agulhas Current system. The South Equatorial Current in Bluelink only flows around the southern tip of Madagascar bypassing the northern tip of Madagascar and ultimately omitting the flow through the Mozambique Channel. This difference in structure explains the lowered transport of Bluelink through the LOCO section compared to MyOcean and HYCOM.

The BTSF structure of the retroflection region is comparable in MyOcean and HYCOM, while Bluelink is different. MyOcean and HYCOM show the flow of the Agulhas Return Current, meandering northward around the Agulhas Plateau, while the flow in Bluelink meanders northward over the Agulhas Plateau. This structural difference is due to the configuration of the numerical model. The numerical model configuration in Bluelink of the flow adjacent to the bathymetry requires further investigation to determine the problem, but is outside the scope of this thesis.

5.1.3 Sea surface height and variability

The analysis of the mean SSH and the standard deviation of SSH shows the overall mean structure and mesoscale variability (standard deviation of SSH acts as a proxy for eddy kinetic energy) of the Agulhas Current System. The mean SSH as a metric, is similar to BTSF, and therefore reinforces the arguments above. The mean SSH especially highlights the incorrect structure of the retroflection region in Bluelink.

The analysis of the mean SSH standard deviation (fig. 4.4) gives an indication of the mesoscale variability represented in the reanalysis products. There are common patterns between the products: high levels of SSH standard deviation in the Mozambique Channel, and south of Madagascar. These features vary slightly in intensity and location, but are common in MyOcean, HYCOM, and Bluelink.

The eddy corridor from the retroflection region into the South Atlantic in MyOcean and HYCOM are comparable, with wide and dissipated pathways into the South Atlantic suggesting variable eddy trajectories. In Bluelink the eddy pathway into the South Atlantic is narrow and concentrated, which is a common error in numerical simulations of the Agulhas Current (Penven et al., 2011). To further investigate the relationship between the numerical models and assimilated data in the reanalysis products the assimilated AVISO SSH is analyzed.

Comparing the SSH standard deviation from the reanalysis products of MyOcean and HYCOM against the AVISO SSH standard deviation reveals the relationship of data assimilation. The SSH mean structure and variability of MyOcean and HYCOM are comparable to AVISO suggesting that the assimilation constrained the reanalysis products to a point. We cannot clearly show to what extent the effect assimilation had when compared to the unassimilated reanalysis products.

Overall the surface structure of the Agulhas Current is well represented in the global reanalysis products from MyOcean and HYCOM. However, Bluelink is unable to adequately simulate the source regions of the Agulhas Current, the retroflection region, and

eddy pathway into the South Atlantic. The ability for data assimilation to constrain the numerical models varies between: different regions of the Agulhas Current System, different metrics plotted, and the reanalysis products indicating no clear pattern.

5.2 Sections

The volume transport through key sections in the Agulhas System (Table 4.1), do not reveal a common pattern between the reanalysis products and the observations. The reanalysis products can overestimate the volume transport upstream (e.g LOCO), while then underestimating the transport further downstream (e.g ACE), or are generally inconsistent with the observations.

This emphasizes the complexity, and non-linearity of the Agulhas Current System and how difficult it is to correctly simulate the region. Moreover there are not necessarily linear relationships between different regions (e.g. Mozambique Channel and Agulhas Current). The transports derived from Eulerian measurements through the GHL section, and the Crossroads section is problematic (van Sebille et al., 2010) due to the high mesoscale variability in the Cape basin (Boebel et al., 2003). The global reanalysis products are investigated with two observational mooring lines (ACE and LOCO), and a proxy was developed to determine the Westward Transport from the Crossroads section.

5.2.1 LOCO

The transport time series from the LOCO section (fig. 4.5) shows a clear seasonal signal, which is reproduced by both the reanalysis products and the observations. This is reinforced by the high correlation values (Table 4.2), and the peak of the power density spectrum at the 3 month frequency (fig. 4.6). The high correlation and seasonal cycle in the transport time series could possibly be caused by either the assimilation of data or the model numerics in the reanalysis products. However the mean and standard deviation values between MyOcean and HYCOM are comparable indicating assimilation successfully constraining the numerical models.

After the seasonal cycle is removed, the correlation is reduced, and the power density spectrum between the reanalysis products and the observations compares poorly.

5.2.2 ACE

In the core of the Agulhas Current, the *in-situ* mooring observations are used to validate the ACE section. MyOcean correctly simulates the volume transport variability (Table 4.3), and correlates well with observations, but underestimates the magnitude. HYCOM correctly simulates the volume transport magnitude and standard deviation, but poorly correlates with the variability of the observations. Both models are unable to accurately simulate the Agulhas Current, displaying errors in different aspects.

The velocity section at ACE shows that MyOcean cannot correctly represent the width and strength of the current compared to the mooring observations, but shows the correct location of the undercurrent. This indicates that the transport is being underestimated possibly due to the incorrect flow structure or weak velocity values.

Even though we cannot directly compare the mean velocity structure from Bluelink to the observations (differing time periods), it is important to note that certain features are represented in Bluelink such as: the undercurrent, V-shape structure, and width of the current (Beal and Bryden, 1999). Unfortunately HYCOM cannot be analyzed due to a lack of velocity data at depth.

5.2.3 Crossroads

The Crossroads section captures the Agulhas Current and Agulhas Return Current, allowing the output of the Agulhas Current System, called the Westward Transport, to be calculated. The method to capture the correct boundaries of the Agulhas Current and Return Current has been completed for MyOcean, but only preliminarily for HYCOM, and Bluelink. Due to the lack of depth velocity data in HYCOM, the boundaries of the Agulhas Current and Agulhas Return Current cannot be correctly troubleshooted. The initial method has been applied to Bluelink, and early troubleshooting shows that 25% of the boundaries of the Agulhas Current and Agulhas Return Current are erroneous.

The results from MyOcean and HYCOM are convincing when compared to current literature as the Westward Transport has similar estimates of Agulhas Leakage (approx. 20 Sv) compared to Richardson (2007). The initial results from Bluelink are encouraging even though 25% are incorrect, the magnitude of the Westward Transport is similar to the estimate from Richardson (2007) of Agulhas Leakage. However, as discussed above there are a number of issues associated with the Bluelink reanalysis product over the Agulhas Current System, and this result above needs to be confirmed.

In Bluelink there is a significant difference between the "total" and "jet" transport over the Crossroads section, which is due to the strong flow through the north faces

of the section. This incorrect flow is most probably due to the incorrect structure of the retroflection region. In the initial troubleshooting process, where each time step of surface velocity, and velocity at depth is analyzed, an early retroflection is frequently observed. This development of such a method to estimate the Westward Transport shows the ability of data assimilated products to be used to perform quantitative research.

Chapter 6

Conclusion

6.1 Concluding summary

Forecasting the ocean is a relatively young discipline in oceanography with the first global initiative of GODAE starting in 1997, and advancing through into GODAE OceanView (Smith and Lefèbvre, 1997; Traon et al., 2009). The global forecast/reanalysis products have improved in spatial resolution so that they are applicable over the regional scale. As there is currently no regional assimilated reanalysis products, reanalysis products from major global prediction systems, are applied to the greater Agulhas Current System.

The reanalysis products (MyOcean, HYCOM and Bluelink) are validated over the greater Agulhas Current System to investigate whether they can adequately simulate the major salient oceanographic features (Lutjeharms, 2006), and investigate the ability of data assimilation to constrain the numerical models through the validation process in MyOcean and HYCOM. The Agulhas Current is difficult to simulate (Penven et al., 2011), impacts global climate (Beal et al., 2011), and is environmentally and economically important for South Africa (Veitch et al., 2010), making it an important system in southern Africa to study.

The validation method is derived from literature (Bryden et al., 2005; Ridderinkhof et al., 2010; Le Bars, 2014), and dynamically important regions in the greater Agulhas Current System (Lutjeharms, 2006). Surface variables are shown and key sections are extracted throughout the region and compared against independent observations and Agulhas Current literature. A Eulerian based method was developed to estimate the Agulhas Leakage, by proxy, by calculating the difference between the volume transport of the Agulhas Current and Agulhas Return Current at the Crossroads section.

The results of this study show that MyOcean and HYCOM represented the salient oceanographic features of the greater Agulhas Current System fairly well, both on the surface and at depth (fig. 6.1). However neither are highly accurate and have minor issues with certain dynamics, which is expected due to the complexity of the Agulhas Current System (Penven et al., 2011). HYCOM is unable to adequately simulate the magnitude of the surface velocity, mesoscale variability of the Agulhas Return Current and the event scale variability in the ACE and LOCO transport time series. MyOcean was unable to sufficiently represent: the magnitude of surface velocity and SSH variability, and the volume transport through ACE. Despite these deficiencies, both MyOcean and HYCOM satisfactorily simulate the salient oceanographic features and variability of the greater Agulhas Current System, and are applicable to the wide array of maritime activities and research occurring in the Agulhas Current System.

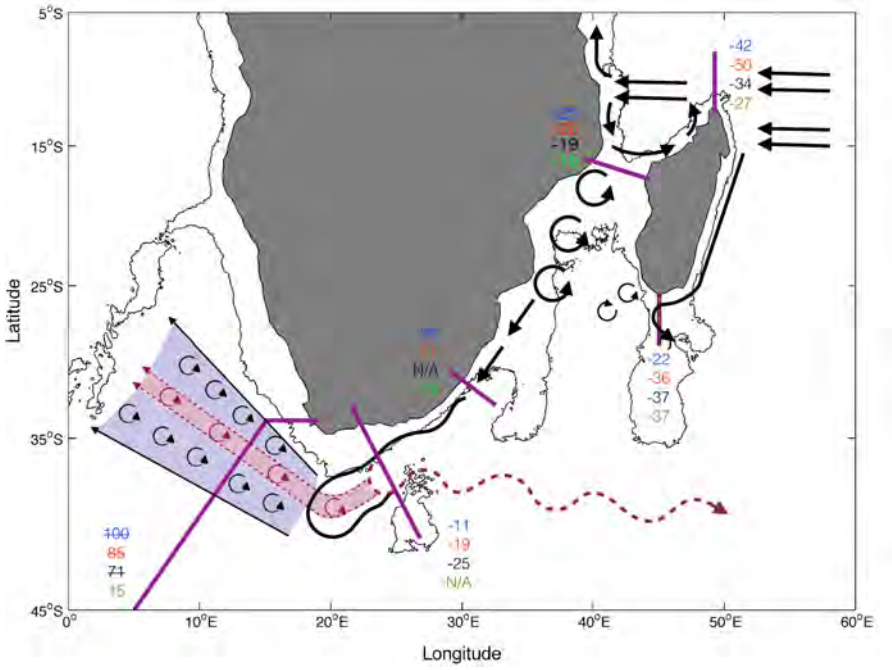

FIGURE 6.1: Summary schematic of the major features, structure and volume transport represented by MyOcean, HYCOM, and Bluelink. Black arrows indicate features/currents in all three reanalysis products while dashed maroon arrow indicates Bluelinks features that deviate from MyOcean and HYCOM. The maroon shaded area indicates the eddy corridor in Bluelink, while light blue represents the eddy corridor in HYCOM and MyOcean. The Volume transport (Sv) through each purple section is given for MyOcean (Blue), HYCOM (red), Bluelink (black) and observations (green)

Bluelink is unable to reproduce the basic salient oceanographic features of the greater Agulhas Current System such as the source and retroflection regions (fig. 6.1). The retroflection region is poorly resolved, and from this analysis we suggest that it is probably due to the configuration of the bathymetric control in the numerical model. The source regions of the greater Agulhas Current System are structurally incorrect with the

South Equatorial Current being misrepresented. Therefore Bluelink would need to be improved before it can be further applied in the greater Agulhas Current System.

Through the validation, the ability of data assimilation to constrain the numerical models is determined for MyOcean and HYCOM. The validation of MyOcean and HYCOM did revealed that the data assimilation managed to somewhat constrain the numerical model as there are clear similarities between the two reanalysis products. However it is difficult to determine whether the numerical model, assimilated data, or assimilation scheme is causing the inconsistencies in the validation.

This thesis forms part of a larger mandate to contribute to developing a regional operational prediction system. This thesis contributes to the current efforts by providing validated simulations that can be used for boundary conditions in the nested prediction system and a rigorous validation method that can used to validate future regional prediction systems.

6.2 Future research

As the current prediction system in Southern Africa is in the early stages of development, and a number of challenges still need to be addressed before a regional prediction system is fully operational. This research needs to be expanded to include the latest product from Mercator Ocean (GLORYS2v3), and the incorrect velocities at depth in the HYCOM product needs to be rectified. The validation needs to be expanded to include daily to weekly time scales that include high frequency dynamics that are important when considering the users and marine stakeholders. Lastly the Eulerian based method to identify the boundaries of the Agulhas Current and Agulhas Return Current at the Crossroads section needs to be performed for both HYCOM and Bluelink.

Beyond this thesis, the methods developed in this study can be applied to a regional hindcast product by Backeberg et al. (2014), and included in a comparative study against the global products. This will allow us to determine the current state of the operational or near-operational regional simulation that is currently being developed. The reanalysis product of Backeberg et al. (2014) needs to be validated as this model provides the initialization for forecasts. The global reanalysis products of MyOcean and HYCOM can possibly be used as the boundary conditions of a regional forecast. Finally the Benguela Current System, which currently lacks any form of data assimilated products, would need to be included in a regional prediction system for Southern Africa.

Bibliography

Ansorge, I. (2014). SAMOC-SA. Technical report, University of Cape Town, Cape Town.

Ansorge, I. J. and Lutjeharms, J. R. E. (2007). The Cetacean Environment off Southern Africa. In Best, P. and Folkens, P. A., editors, *Whales and Dolphins of the Southern African subregion*, pages 1–13. Cambridge University Press.

Ansorge, I. J., Speich, S., Froneman, P. W., Rouault, M., and Garzoli, S. (2005). Monitoring the oceanic flow between Africa and Antarctica: Report of the first GoodHope cruise. *South African Journal of Science*, (February):29–35.

Argo Science Team (2001). Argo: The global array of profiling floats. In Koblinsky, C. and Smith, N., editors, *Observing the Oceans in the 21st Century*.

Backeberg, B. (2008). The greater Agulhas Current system: An integrated study of its mesoscale variability. *Journal of ...*, 1(1):29–44.

Backeberg, B., Counillon, F., and Johannessen, J. (2014). Assimilating along-track SLA data using the EnOI in an eddy resolving model of the Agulhas system. *Ocean Dynamics*.

Backeberg, B. C., Bertino, L., and Johannessen, J. a. (2009). Evaluating two numerical advection schemes in HYCOM for eddy-resolving modelling of the Agulhas Current. *Ocean Science Discussions*, 6(1):429–475.

Beal, L. and Bryden, H. (1997). Observations of an Agulhas Undercurrent. *Deep Sea Research Part I: Oceanographic Research Papers*, 44(9):1715–1724.

Beal, L. and Bryden, H. (1999). The velocity and vorticity structure of the Agulhas Current at 32 S. *Journal of Geophysical Research: ...*, 104(1998):5151–5176.

Beal, L. M., De Ruijter, W. P. M., Biastoch, A., and Zahn, R. (2011). On the role of the Agulhas system in ocean circulation and climate. *Nature*, 472(7344):429–36.

Biastoch, a., Böning, C. W., Schwarzkopf, F. U., and Lutjeharms, J. R. E. (2009). Increase in Agulhas leakage due to poleward shift of Southern Hemisphere westerlies. *Nature*, 462(7272):495–8.

Biastoch, A. and Krauss, W. (1999). The role of mesoscale eddies in the source regions of the Agulhas Current. *Journal of Physical Oceanography*, 29(9):2303–2317.

Biastoch, a., Lutjeharms, J. R. E., Böning, C. W., and Scheinert, M. (2008). Mesoscale perturbations control inter-ocean exchange south of Africa. *Geophysical Research Letters*, 35(20):L20602.

Bleck, R. (2002). An oceanic general circulation model framed in hybrid isopycnic-Cartesian coordinates. *Ocean Modelling*, 4(1):55–88.

Boebel, O., Lutjeharms, J., and Schmid, C. (2003). The Cape Cauldron: a regime of turbulent inter-ocean exchange. *Deep Sea Research ...*, 50:57–86.

Bronez, T. P. (1992). On the Performance Advantage of Multitaper Spectral Analysis. *IEEE TRANSACTIONS ON SIGNAL PROCESSING*, 40(12).

Bryden, H., Beal, L., and Duncan, L. (2005). Structure and transport of the Agulhas Current and its temporal variability. *Journal of Oceanography*, 61(1980):479–492.

Collins, C., Hermes, J., and Reason, C. (2014). Mesoscale activitiy in the Comoros Basin from satellite altimetry and a high-resolution ocean circulation model. *Journal of Geophysical Research: Oceans*.

Cummings, J. A. and Smedstad, O. M. (2013). *Data Assimilation for Atmospheric, Oceanic and Hydrologic Applications (Vol. II)*, volume II. Springer Berlin Heidelberg, Berlin, Heidelberg.

Deshayes, J., Curry, R., and Msadek, R. (2014). CMIP5 Model Intercomparison of Freshwater Budget and Circulation in the North Atlantic. *Journal of Climate*, 27(9):3298–3317.

Durgadoo, J. V., Loveday, B. R., Reason, C. J. C., Penven, P., and Biastoch, A. (2013). Agulhas Leakage Predominantly Responds to the Southern Hemisphere Westerlies. *Journal of Physical Oceanography*, 43(10):2113–2131.

Goni, G., Roemmich, D., Molinari, R., Meyers, G., Sun, C., Boyer, T., Baringer, M., Gouretski, V., Dinezio, P., Reseghetti, F., Vissa, G., Swart, S., Keeley, R., Garzoli, S., Rossby, T., Maes, C., and Reverdin, G. (2009). The ship of opportunity program. In Hall, J., Harrison, D. E., and D, S., editors, *OceanObs'09: sustained ocean observations and information for society*, number 1, Venice, Italy.

Gründlingh, M. L. (1983). On the Course of the Agulhas Current. *South African Geographical Journal*, 65(1).

Hall, C. and Lutjeharms, J. (2011). Cyclonic eddies identified in the Cape Basin of the South Atlantic Ocean. *Journal of Marine Systems*, 85(1-2):1–10.

International GODAE Steering Team (2000). The global ocean data assimilationexperiment strategic plan. Technical report, GODAE.

Le Bars, D. (2014). *Dynamics and estimation of the Agulhas leakage*. PhD thesis, Utrecht University.

Loveday, B. (2014). Decoupling of the Agulhas leakage from the Agulhas Current. *Journal of Physical ...*, 44(7):1776–1797.

Lutjeharms, J. and Ansorge, I. (2001). The Agulhas Return Current. *Journal of Marine Systems*, 30(1-2):115–138.

Lutjeharms, J., Bang, N., and Duncan, C. (1981). Characteristics of the currents east and south of Madagascar. *Deep Sea Research Part A. Oceanographic Research Papers*, 28(9).

Lutjeharms, J. and Roberts, H. R. (1988). The Natal Pulse: An Extreme Transient on the Agulhas Current. *Journal of Geophysical Research*, 93:631–645.

Lutjeharms, J. R. E. (2006). *The Agulhas Current*. Springer.

Lutjeharms, J. R. E. and Cooper, J. (1996). Interbasin leakage through Agulhas current filaments. *Deep Sea Research Part I: Oceanographic Research Papers*, 43(2).

Mcphaden, M. J., Ando, K., Freitag, H. P., Lumpkin, R., Masumoto, Y., Murty, V. S. N., Ravichandran, M., Vialard, J., Vousden, D., and Yu, W. (2009). The global tropical moored buoy array. In Hall, J., Harrison, D. E., and D, S., editors, *OceanObs'09: sustained ocean observations and information for society*, number 1, Venice, Italy.

Metzger, J. E., Smedstad, O. M., Thoppil, P. G., Hurlburt, H. E., Cummings, J. A., Wallcraft, A. J., Zamudio, L., Franklin, D. S., Posey, P. G., Phelps, M. W., Hogan, P. J., Bub, F. L., and DeHaan, C. J. (2014). US Navy Operational Global Ocean and Arctic Ice Prediction Systems. *Oceanography*, pages 1–22.

MyOcean (2013). GLOBAL OCEAN PHYSICS RENANLYSIS GLORYS2V1. Technical Report April, Mercator Ocean.

Nauw, J. J., van Aken, H. M., Webb, a., Lutjeharms, J. R. E., and de Ruijter, W. P. M. (2008). Observations of the southern East Madagascar Current and undercurrent and countercurrent system. *Journal of Geophysical Research*, 113(C8):C08006.

OceanSAfrica (2012). OceanSAfrica : Developing Operational Oceanography Capabilities for Africa. Technical Report July, OceanSAfrica.

Oke, P., Griffin, D., and Schiller, A. (2013). Evaluation of a near-global eddy-resolving ocean model. *Geoscientific model ...*, 6(3):591–615.

Oke, P. R. (2002). Assimilation of surface velocity data into a primitive equation coastal ocean model. *Journal of Geophysical Research*, 107(C9):3122.

Parent, L., Ferry, N., Barnier, B., and Garric, G. (2013). GLOBAL Eddy-Permitting Ocean Reanalyses and Simulations of the period 1992 to Present. Technical report, Mercator Ocean.

Penven, P., Herbette, S., and Mathieu, R. (2011). Ocean Modelling in the Agulhas Current System. Technical report, Nansen-Tutu Centre for Marine and Environmental Research, Cape Town.

Penven, P., Lutjeharms, J. R. E., and Florenchie, P. (2006). Madagascar: A pacemaker for the Agulhas Current system? *Geophysical Research Letters*, 33(17):L17609.

Richardson, P. L. (2007). Agulhas leakage into the Atlantic estimated with subsurface floats and surface drifters. *Deep Sea Research Part I: Oceanographic Research Papers*, 54(8):1361–1389.

Ridderinkhof, H. and de Ruijter, W. (2003). Moored current observations in the Mozambique Channel. *Deep Sea Research Part II: Topical Studies in Oceanography*, 50(12-13):1933–1955.

Ridderinkhof, H., van der Werf, P. M., Ullgren, J. E., van Aken, H. M., van Leeuwen, P. J., and de Ruijter, W. P. M. (2010). Seasonal and interannual variability in the Mozambique Channel from moored current observations. *Journal of Geophysical Research*, 115(C6):C06010.

Rouault, M., Mouche, A., Collard, F., Johannessen, J., and Chapron, B. (2010). Mapping the Agulhas Current from space: An assessment of ASAR surface current velocities. *Journal of Geophysical Research*, 115(C10):C10026.

Sæ tre, R. and Da Silva, A. J. (1984). The circulation of the Mozambique channel. *Deep Sea Research Part A. Oceanographic Research Papers*, 31(5):485–508.

Schiller, A. and Brasssington, G. B., editors (2011). *Operational Oceanography in the 21st Century*. Springer.

Schouten, M. W., Ruijter, W. P. M. D., and Leeuwen, P. J. V. (2002). Upstream control of Agulhas Ring shedding. *Journal of Geophysical Research: Oceans*, 107(August).

Smith, N. and Lefèbvre, M. (1997). The Global Ocean Data Assimilation Experiment (GODAE). In *Monitoring the Oceans in the 2000s: An Integrated Approach*, Biarritz, France.

Stewart, R. H. (2008). *Introduction to Physical Oceanography*. Department of Oceanography, Texas A & M Unversity, Texas.

Swallow, J., Fieux, M., and Schott, F. (1988). The Boundary Currents East and North of Madagascar 1. Geostrophic Currents and Transports. *Journal of Geophysical Research*, 93(7):4951–4962.

Traon, P. Y. L., Bell, M., Dombrowsky, E., Schiller, A., and Wilmer-Becker, K. (2009). GODAE OceanView : from an experiment towards a long-term Ocean Analysis and Forecasting International Program. In Hall, J., Harrison, D. E., and D, S., editors, *OceanObs'09: sustained ocean observations and information for society*, number 1, Venice, Italy.

van Ballegooyen, R. C., Diedericks, G., Rossouw, M., Meyer, A., Terblanche, L., and de Wet, P. (2011). High resolution and multi-disciplinary coastal system modelling to meet stakeholder needs. Technical report, Nansen-Tutu Centre for Marine Environmental Research, Cape Town.

van Sebille, E., Barron, C. N., Biastoch, a., van Leeuwen, P. J., Vossepoel, F. C., and de Ruijter, W. P. M. (2009). Relating Agulhas leakage to the Agulhas Current retroflection location. *Ocean Science Discussions*, 6(2):1193–1221.

van Sebille, E., van Leeuwen, P. J., Biastoch, A., and de Ruijter, W. P. (2010). Flux comparison of Eulerian and Lagrangian estimates of Agulhas leakage: A case study using a numerical model. *Deep Sea Research Part I: Oceanographic Research Papers*, 57(3):319–327.

Veitch, J., Backeberg, B., and Shillington, F. (2010). SimOcean: modelling the ocean. *SANCOR Newsletter*, (June):16 – 17.